U.S. Army Coast. Eng. Res. Ctr. Tech. Rep. CERC-86-8
Sep 1986

US Army Corps of Engineers

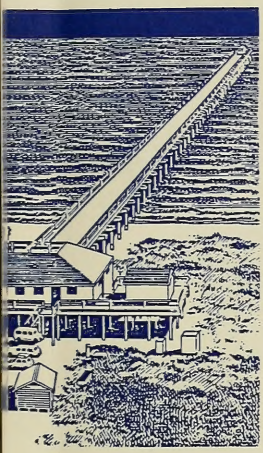

GB
450
.T45
no. CERC-
86-8

TECHNICAL REPORT CERC-86-8

FREQUENCY OF COASTAL FLOODING AT ROUGHANS POINT, BROAD SOUND, LYNN HARBOR, AND THE SAUGUS-PINES RIVER SYSTEM

by

Thomas A. Hardy, Peter L. Crawford

Coastal Engineering Research Center

DEPARTMENT OF THE ARMY
Waterways Experiment Station, Corps of Engineers
PO Box 631, Vicksburg, Mississippi 39180-0631

September 1986
Final Report

Approved For Public Release; Distribution Unlimited

DOCUMENT
LIBRARY
Woods Hole Oceanographic
Institution

Prepared for

US Army Engineer Division, New England
Waltham, Massachusetts 02254-9149

Destroy this report when no longer needed. Do not return it to the originator.

The findings in this report are not to be construed as an official Department of the Army position unless so designated by other authorized documents.

The contents of this report are not to be used for advertising, publication, or promotional purposes. Citation of trade names does not constitute an official endorsement or approval of the use of such commercial products.

Unclassified

SECURITY CLASSIFICATION OF THIS PAGE

REPORT DOCUMENTATION PAGE

Form Approved OMB No. 0704-0188 Exp. Date: Jun 30, 1986

1a. REPORT SECURITY CLASSIFICATION: Unclassified

1b. RESTRICTIVE MARKINGS:

2a. SECURITY CLASSIFICATION AUTHORITY:

2b. DECLASSIFICATION / DOWNGRADING SCHEDULE:

3. DISTRIBUTION / AVAILABILITY OF REPORT: Approved for public release; distribution unlimited

4. PERFORMING ORGANIZATION REPORT NUMBER(S): Technical Report CERC-86-8

5. MONITORING ORGANIZATION REPORT NUMBER(S):

6a. NAME OF PERFORMING ORGANIZATION: USAEWES, Coastal Engineering Research Center

6b. OFFICE SYMBOL (If applicable): WESCV

7a. NAME OF MONITORING ORGANIZATION:

6c. ADDRESS (City, State, and ZIP Code): PO Box 631, Vicksburg, MS 39180-0631

7b. ADDRESS (City, State, and ZIP Code):

8a. NAME OF FUNDING / SPONSORING ORGANIZATION: US Army Engineer Division, New England

8b. OFFICE SYMBOL (If applicable):

9. PROCUREMENT INSTRUMENT IDENTIFICATION NUMBER:

8c. ADDRESS (City, State, and ZIP Code): 424 Trapelo Road, Waltham, MA 02254-9149

10. SOURCE OF FUNDING NUMBERS

PROGRAM ELEMENT NO.	PROJECT NO.	TASK NO.	WORK UNIT ACCESSION NO

11. TITLE (Include Security Classification): Frequency of Coastal Flooding at Roughans Point, Broad Sound, Lynn Harbor, and the Saugus-Pines River System

12. PERSONAL AUTHOR(S): Hardy, Thomas A., Crawford, Peter L.

13a. TYPE OF REPORT	13b. TIME COVERED	14. DATE OF REPORT (Year, Month, Day)	15. PAGE COUNT
Final report	FROM May 1984 TO Dec 1985	September 1986	98

16. SUPPLEMENTARY NOTATION: Available from National Technical Information Service, 5285 Port Royal Road, Springfield, VA 22161

17. COSATI CODES		
FIELD	GROUP	SUB-GROUP

18. SUBJECT TERMS (Continue on reverse if necessary and identify by block number): Coastal flooding; Wave overtopping; Storm surge; Flood frequency; Stage-frequency

19. ABSTRACT (Continue on reverse if necessary and identify by block number)

This report describes the establishment of frequency curves for water levels caused by the combination of tide, storm surge, and waves for a coastal area just north of Boston. The project procedure involves the conjunctive use of five modeling components, including numerical storm surge, numerical wave propagation, physical wave overtopping, flood routing, and probability models.

At Roughans Point where flooding is caused by the overtopping of seawalls by storm waves, all five models were necessary. Multiple combinations of possible seawall-revetment structures were modeled. Major differences among the combinations were evident at the lower return periods with the combinations of a wide berm revetment and a cap on the existing seawall for the east wall of Roughans Point providing the greatest protection. At higher return periods the protection differential offered by the various structure combinations tended to diminish. For still-water levels and wave conditions of a Standard Project

(Continued)

20. DISTRIBUTION / AVAILABILITY OF ABSTRACT: ☒ UNCLASSIFIED/UNLIMITED ☐ SAME AS RPT. ☐ DTIC USERS

21. ABSTRACT SECURITY CLASSIFICATION: Unclassified

22a. NAME OF RESPONSIBLE INDIVIDUAL:

22b. TELEPHONE (Include Area Code):

22c. OFFICE SYMBOL:

DD FORM 1473, 84 MAR — 83 APR edition may be used until exhausted. All other editions are obsolete.

SECURITY CLASSIFICATION OF THIS PAGE: Unclassified

MBL/WHOI

0 0301 0091254 9

20. ABSTRACT (Continued)

Northeaster all structure combinations tested would be ineffective at protecting the interior of Roughans Point. Tests were conducted to determine a structure height for the north wall. These tests indicated that significant overtopping did not begin until the north wall structure was lowered below 13 ft National Geodetic Vertical Datum (NGVD). Since the existing height of the north wall is above this level at several sections, it is recommended that the revetment height be set at 13 ft NGVD with the wall height set so that there is a transition between the existing wall heights.

For areas where stage-frequency curves are presented for the still-water level resulting from the combination of storm surge and astronomical tide, only the storm surge and probability models were necessary. These areas include both open coast and estuarine locations. For areas flooded by the still-water level, results of the modeling indicated that the whole study area floods to approximately the same level. Flood levels are efficiently conveyed through the inlet and throughout the flood plain of the Saugus-Pines River system. Inside the inlet, there is a small gradient in the still-water level, rising from north to south, which results from local setup caused by north to northeast wind directions which predominate during storm conditions. This local wind setup results in flood levels inside the inlet which differ by one-half to three-fourths of a foot during the more severe storm events. Outside the river system in Broad Sound a smaller north-south gradient exists with differences of only a few tenths of a foot resulting. Data collected by the US Army Engineer Division, New England, after completion of the modeling indicated that losses do occur as flood levels propagate upstream of the Fox Hill Drawbridge on the Saugus River and upstream of the Highway embankment on the Pines River. Stage-frequency curves for these areas were adjusted to accommodate these additional data. The curves were lowered 0.3 and 0.5 ft at the lower return periods for upstream Saugus River and Pines River locations, respectively. Reductions were reduced for higher return periods because higher flood levels would provide greater access of floodwaters to these areas.

The setup and operation of all models, except the physical model, are described. The method of constructing stage-frequency curves is explained, and estimates of the error involved in each of the processes are discussed. The final products are curves which relate flood stage to frequency of occurrence for several possible structures at Roughans Point as well as for several coastal and river areas.

PREFACE

The US Army Engineer Division, New England (NED) requested the US Army Engineer Waterways Experiment Station (WES) Coastal Engineering Research Center (CERC) to conduct numerical and physical model studies to determine the frequency of flood levels at Roughans Point and at other coastal areas in Revere, Saugus, and Lynn, Massachusetts. The studies were conducted principally to provide greater confidence in the flood protection plan for Roughans Point as presented in the planning report (NED 1983) and were part of a larger study, "Continuing Planning and Engineering Studies for Roughans Point," provided for under the 12 September 1969 Southeastern New England authorization of the US Senate Committee on Public Works. A small funding contribution came from Revere Backshore planning studies conducted under the same authority.

This report contains the results of the numerical investigations conducted between May 1984 and December 1985. Close consultation and cooperation were maintained between CERC and NED throughout the study, and the efforts of Mr. Charles Wener, NED, were particularly important in its successful completion.

Work was performed by personnel of the Research Division (CR), CERC, under the direction of Dr. James R. Houston, former Chief, CR. Mr. Thomas A. Hardy, Coastal Processes Branch (CR-P), was the Principal Investigator for this study under the direction of Mr. H. Lee Butler, former Chief, CR-P, and current Chief, CR. Mr. Hardy was responsible for the probability modeling, storm surge modeling, flood routing, and synthesis of the total modeling effort. Mr. Peter L. Crawford, Coastal Oceanography Branch (CR-O), was responsible for the wave modeling. Mr. Crawford worked under the direction of Dr. E. F. Thompson, Chief, CR-O. Upon completion of the study, Chief and Assistant Chief, CERC, were Dr. Houston and Mr. Charles C. Calhoun, Jr., respectively. This report was edited by Ms. Shirley A. J. Hanshaw, Information Products Division, Information Technology Laboratory, WES.

COL Allen F. Grum, USA, was the previous Director of WES. COL Dwayne G. Lee, CE, is the present Commander and Director. Dr. Robert W. Whalin is Technical Director.

CONTENTS

	Page
PREFACE	1
CONVERSION FACTORS, NON-SI TO SI (METRIC) UNITS OF MEASUREMENT	3
PART I: INTRODUCTION	4
Terminology	7
Overview of Project Technique	8
Organization of Report	10
PART II: PROBABILITY MODEL	11
Choosing Storm Surge Time-Histories	12
Creating Synthetic Surge Plus Tide Events	14
Selecting Events to Model	15
PART III: STORM SURGE PLUS TIDE SIMULATION	23
Grid Development	23
Wind Forcing	24
Data Collection	25
Model Calibration	25
Model Verification	30
Simulation of Event Ensemble by the Hydrodynamic Model	30
PART IV: WAVE MODELING	38
WIS Methods and Data	40
Phase III Methodology	40
Use of Phase III Methodology for Broad Sound Wave Climate Simulations	41
Wave Climate Simulations for Broad Sound	42
ESCUBED Results	44
Locally Generated Waves in the Lee of Nahant Peninsula	44
PART V: FLOOD STAGES FOR THE INTERIOR OF ROUGHANS POINT	50
Overtopping Rate Calculation	55
Flood Routing	57
Simulation of the Event Ensemble by the Flood Routing Model	63
North Wall Tests	64
PART VI: STAGE-FREQUENCY CURVES	66
PART VII: RESULTS AND CONCLUSIONS	68
Roughans Point	68
Still-Water Locations	72
Estimating Error in the Frequency Curves	82
Determining Error Bands for the Selection Process	85
Assessing the Impact of the Standard Project Northeaster	89
Conclusions	92
REFERENCES	94

CONVERSION FACTORS, NON-SI TO SI (METRIC)
UNITS OF MEASUREMENT

Non-SI units of measurement used in this report can be converted to SI (metric) units as follows:

Multiply	By	To Obtain
acres	4,046.873	square meters
cubic feet per second	0.02831685	cubic meters per second
feet	0.3048	meters
knots (international)	1.8532	kilometers per hour
miles (US statute)	1.609344	kilometers
square miles (US statute)	2.589988	square kilometers

FREQUENCY OF COASTAL FLOODING AT ROUGHANS POINT, BROAD SOUND, LYNN HARBOR, AND THE SAUGUS-PINES RIVER SYSTEM

PART I: INTRODUCTION

1. The study area was located in the cities of Revere, Lynn, and Saugus, Massachusetts, which are immediately north of Boston. Roughans Point (Figure 1) is a 55-acre* residential area which is below the elevation of a spring tide at many locations. Seawalls along both the northern and eastern boundaries offer some protection against coastal flooding. However, damage resulting from flooding caused when waves overtop the seawalls is a frequent occurrence. The Saugus and Pines Rivers join just before passing under the General Edwards Bridge and out into Broad Sound. The lower 2,500 acres of the drainage area just behind Revere Beach are mostly river channel and marsh. This area borders residential, commercial, and industrial areas, many of which are at an elevation only a few feet greater than the elevation of the maximum astronomical tide. Flooding is caused by the inundation of low lying areas by the combination of astronomical tide and storm surge. The Revere Beach-Point of Pines-Lynn Harbor region is made up of recreational beaches, residential and industrial land protected by seawalls, and harbor areas. Flooding results from overtopping of seawalls and dunes by storm waves. Figure 2 is a map of the study area vicinity showing the above locations.

2. The desired products of this project are stage-frequency curves which relate the elevation of floodwaters to the average waiting time between floods of equal or greater severity. The ordinate of these curves is stage, measured in feet above the National Geodetic Vertical Datum (NGVD), and the abscissa is return period expressed in years. The primary goal of this study initially was to provide flood frequencies at Roughans Point where flooding is caused by the overtopping of seawalls by storm waves. The numerical model efforts needed to predict waves and water levels at Roughans Point could also predict these quantities at nearby locations. Therefore, the scope of the project was expanded to provide flood frequencies for the Saugus-Pines River

---

* A table of factors for converting non-SI units of measurement to SI (metric) units is presented on page 3.

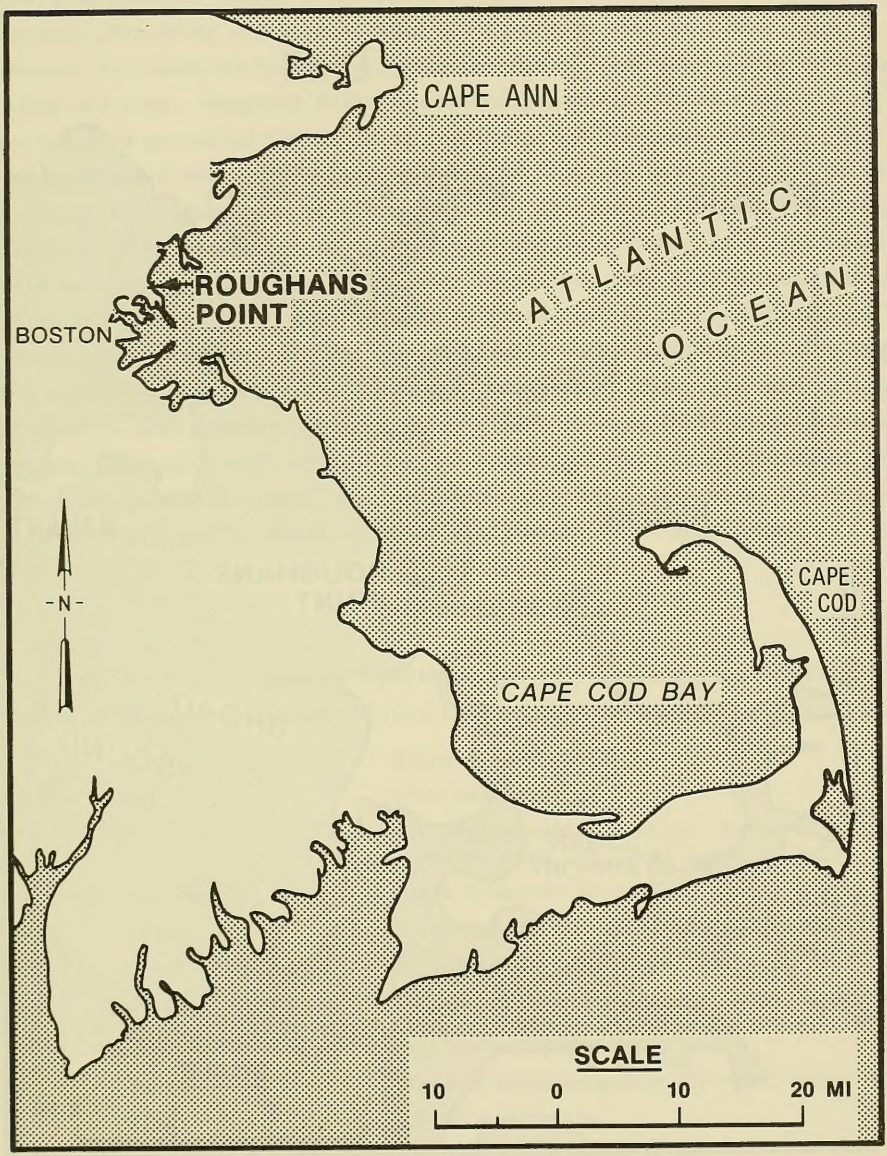

Figure 1. Location of study area

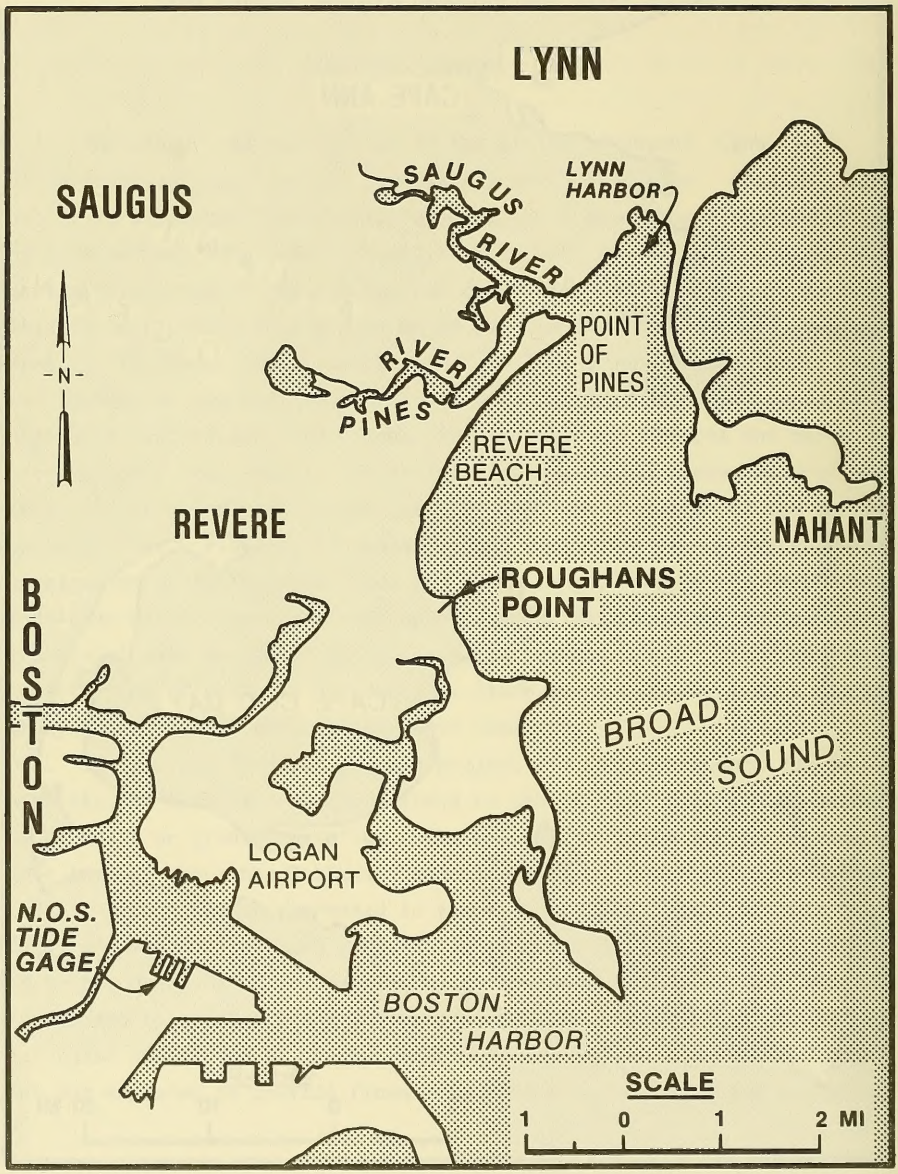

Figure 2. Study area vicinity

System, as well as wave and water level information, and techniques which could be used for future overtopping studies at Point of Pines and Lynn Harbor. The study was then divided into two main sections, determined by whether the cause of the water levels was due to wave overtopping or combined surge and tide. Roughans Point was the only location where stage-frequency curves were generated for flooding resulting from wave overtopping. For the Saugus-Pines River System, flooding results from the inundation of low lying areas by the combination of storm surge and astronomical tide. Even though flooding at Revere Beach, Point of Pines, and Lynn Harbor is caused mostly by wave overtopping, only the still-water level frequency will be reported because the present study did not include investigation of overtopping for these areas. Wave overtopping for these areas will be estimated by US Army Engineer Division, New England (NED), in other studies using techniques and data developed by US Army Engineer Waterways Experiment Station (WES) Coastal Engineering Research Center (CERC) for the present study. Areas where the stage-frequency curves are based upon combined surge and tide levels, but include no wave effects, will be referred to as still-water level locations.

Terminology

3. To avoid excessive repetition and to provide greater clarity, the following terms are defined for use throughout this report.

Event	Storm plus tide
MSL	Mean sea level
NGVD	National Geodetic Vertical Datum (formerly called mean sea level datum of 1929)
Northeaster	Extra-tropical storm
Stage	Elevation of the still-water level above NGVD
Still-water Level	Elevation of surge plus tide water surface
Storm	The historical meteorology (wind, waves, and surge) independent of the tide with which it actually occurred
Surge	Storm-induced component of still-water level
Tide	Astronomical tide

Overview of Project Technique

4. The establishment of frequency curves required the conjunctive use of several modeling components. At Roughans Point the combined use of probability, numerical storm surge, numerical wave, physical, and flood routing models was required to produce the stage-frequency curves. Whereas, for the still-water locations (Saugus-Pines River and Revere Beach-Lynn Harbor areas) only the probability and numerical storm surge models were required. The following is a brief description of each model.

5. The probability model was designed to complete four tasks: select events for simulation by the other models, assign probabilities to these events, create stage-frequency curves, and determine a measure of confidence in the final results. The numerical storm surge model simulated the storm plus tide events producing a time-history of still-water levels at specific locations throughout the study area. A numerical, spectral wave model simulated the wave field which accompanied each of the events simulated by the storm surge model. Also, a monochromatic wave model estimated the locally generated waves which were not considered in the spectral model. The wave parameters of height, period, and direction were calculated at selected sites throughout the study area. The physical model determined coefficients for an overtopping rate equation by testing multiple combinations of water level and spectral wave characteristics for several existing and proposed structures at Roughans Point. The physical modeling is not fully described in this report. (For complete details of the physical modeling see Ahrens and Heimbaugh (in preparation). The flood routing model calculated the maximum stage in the interior of Roughans Point caused by each event. Maximum stage was determined after outflows from drainage, pumping, seepage, and weir flow over low lying boundaries were considered.

6. Figure 3 is a flow chart which depicts the conjunctive use of the above models for the establishment of stage-frequency curves. Basically, the probability model selected and assigned probability to the surge-tide-wave events simulated. Then, the surge model simulated the still-water level. At this point stage-frequency curves were generated for the still-water locations. To develop the flood levels caused by wave overtopping at Roughans Point, the wave, physical, and flood routing models were necessary. The wave model simulated the parameters, height, period, and direction. The output of

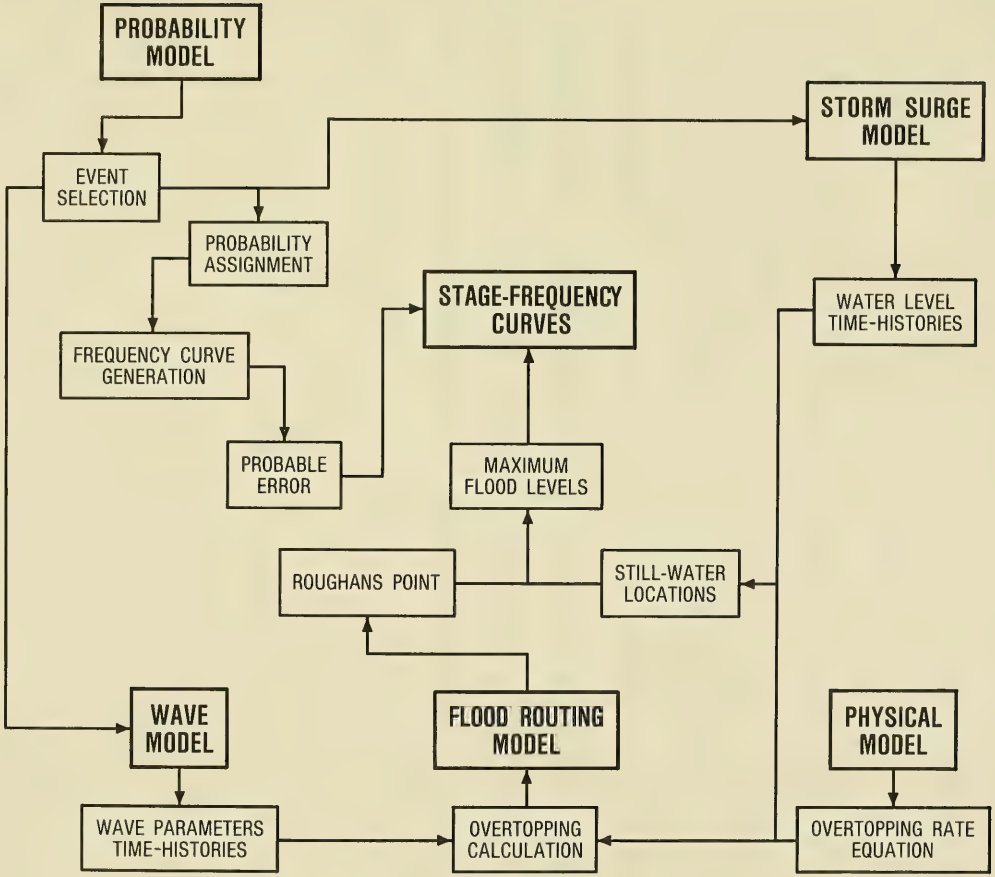

Figure 3. Flow chart of project technique

the two numerical models (surge and wave) were the main inputs to the physical model's overtopping rate equation which produced the overtopping rate for each required time-step. The water volume due to overtopping was then routed through the Roughans Point area, and a maximum stage was calculated for each event. Finally, a stage-frequency curve was created for flood levels induced by wave overtopping.

Organization of Report

7. This report is structured as follows. Part II is a description of the probability model. Modeling of the surge plus tide events is discussed in Part III, including calibration and verification of the storm surge model. Part IV is a description of the numerical wave modeling. The methods for calculating the overtopping rate time-histories and routing the flood through Roughans Point are discussed in Part V. The construction of stage-frequency curves is explained in Part VI. Part VII contains discussion of the results, including an estimate of the error in the stage-frequency curves. Because of the large volume of results generated by the numerical models, time-histories of ocean water levels, waves, winds, overtopping rates, and Roughans Point interior flood levels are not provided in this report but were given to NED on computer tape.

PART II: PROBABILITY MODEL

8. Unlike the physical model which simulates a physical process with physical operations and the numerical models which simulate physical processes with mathematical operations, the probability model does not simulate a physically realizable entity. The title 'model' is used for symmetry with the other components of this project. The probability model is essentially an assemblage with four specific tasks: select events for simulation by the other three models, assign probabilities to these events, create stage-frequency curves, and determine a measure of confidence in these curves.

9. Ideally, there would be a long historical data record of the desired quantity at the desired location (for example, 100 years of overtopping data at Roughans Point). For this ideal case modeling would not be necessary. An overtopping rate frequency curve could be created using well-established statistical techniques which can be found in any hydrology text. However, as is usually the case, sufficient data records for the quantities of interest were not available. Therefore, three separate modeling efforts, a physical overtopping model, a numerical storm surge model, and a numerical wave model were implemented to overcome the lack of data.

10. There are several possible approaches in establishing frequency curves where the scarcity of data in the immediate study area requires a modeling approach. The two most common are called the historical method and the joint probability method (JPM). In the historical method, a series of historical events is recreated with the pertinent data being saved in the necessary locations. In effect, it is like operating a time machine with the hindsight to know what data to collect and where to collect it. Probability is assigned to each event by a standard ranking method. For the JPM, the storm type is parameterized. For example, hurricane wind fields can be defined by three parameters, central pressure deficit, radius to maximum winds, and forward speed. Then, an ensemble of synthetic events is simulated representing those events which are possible in the study area. Probability is assigned to individual events by assigning probabilities to parameter values which determine that event. If the parameters are independent, then the probability of the event would be the product of the probabilities of the component parameters. Several studies have been conducted using the above two methods, including Meyers (1970) and Prater, Hardy, and Butler (in preparation). For the present

study, since hurricanes do not significantly contribute to stage-frequencies in the project area, and since northeasters are difficult to parameterize, a modification of the historical approach was used. Historical storm surge time-histories were combined randomly with tide time-histories to produce synthetic event water level time-histories. Probabilities were assigned using data from a nearby tide gage. This process is explained in detail in the following paragraphs.

Choosing Storm Surge Time-Histories

11. Regardless of the approach selected, data in the vicinity of the study area are essential for identifying inputs to the numerical modeling and for assigning probabilities. This project was fortunate in having convenient sources for the necessary data. The National Ocean Service's (NOS's) Boston tide gage has been in continuous service since 1922. This gage is located at Commonwealth Pier in Boston Harbor which is less than 5 miles from the study area. Wave hindcast information was available for deep water adjacent to the study area from the WES Wave Information Study (WIS). Hourly wind data were available from Logan International Airport which is less than 5 miles from the study area. The 20-year period from 1956-1975 was chosen from which to gather data for use in the numerical modeling. This period was selected because information was available from the above mentioned sources in all the necessary data categories: water level, wind, and wave.

12. By defining storm surge as the difference between measured water level and predicted tide, a partial duration series of storm surge time-histories (26 storms) was extracted from the Boston tide gage data. A minimum value of the maximum surge, 2.5 ft, was used to define those storms which had a reasonable probability of causing significant flooding. If surges much below the 2.5-ft level were combined with possible tides, it would be unlikely that any of the resulting events would be selected as one of the relatively small number of events to be modeled (only 150 events with water levels from 7.9 to 11.2-ft NGVD were selected). The value of 2.5 ft was chosen using the following guidance: with this surge level, only 5 percent (Harris 1981) of the hourly tide heights are high enough so that the combined surge plus tide would be greater than 7.9 ft NGVD. The combination of surge and tide and the selection of the events to be modeled are explained later in this report.

13. Two additional storms from outside the 1956-1975 period were included in the storm ensemble: 29 November 1945 and 6 February 1978. All the necessary data were obtainable for these storms which caused the first and second highest surges recorded at Boston. Furthermore, the February 1978 event caused the highest still-water level (10.3 ft NGVD) on record in Boston. Adding these two storms helped ensure the top end of the storm ensemble was representative of what could occur at Boston. Therefore, a total of 28 storms was chosen to represent the surge time-histories which are possible at Boston. Table 1 contains a list of these storms and their maximum surges. The maximum surges listed in Table 1 might differ slightly from maximum surges derived elsewhere. There are two reasons for these small discrepancies. First, great care was taken to use a set of tidal prediction constituents which best fits the tidal signal at Boston. With the large tidal range at Boston, slight errors in phase could cause significant errors in the calculated surge. Five separate sets of constituents received from NOS were tested, and the set of constituents with the best fit was used for these calculations. Second, often the maximum surge in historical storms occurs at low water because of the increase in surge with decreasing water level given constant wind speed and direction. Since the surges needed to be independent of their historic tide, the surge time-histories were edited by eye to remove 12-hour oscillations caused by this shallow-water effect.

Table 1

Historical Storms Chosen to Represent Possible Surges at Boston

Storm No.	Date	Maximum Surge ft	Storm No.	Date	Maximum Surge ft
1	11-30-45	4.8	15	4-13-61	4.4
2	1-9-56	3.3	16	3-7-62	2.5
3	3-16-56	3.3	17	12-6-62	2.7
4	4-8-56	2.6	18	2-19-64	2.7
5	1-8-58	2.9	19	1-23-66	3.1
6	1-15-58	2.7	20	1-30-66	3.6
7	2-16-58	3.6	21	12-25-66	2.9
8	3-15-58	2.8	22	2-9-69	3.4
9	3-21-58	3.2	23	12-27-69	3.2
10	4-2-58	2.7	24	2-4-72	2.9
11	12-29-59	2.6	25	2-19-72	4.0
12	2-19-60	2.5	26	11-9-72	2.8
13	3-4-60	3.7	27	12-16-72	3.2
14	1-20-61	3.4	28	2-6-78	4.7

Creating Synthetic Surge Plus Tide Events

14. Since the tidal range at Boston (mean range--9.5 ft and maximum range--14.6 ft) is much larger than the largest recorded surge (approximately 5 ft), the tide is a very important component of the total water level. Rather than numerically model the relatively small sample of historical events (surge plus tide), synthetic events were created by combining the historical storm surge time-histories with possible tide time-histories. The basic assumption behind this technique is that the surge time-history (edited to remove the shallow-water effect) of any storm is independent of the tide with which it occurs. In other words, the phenomena which cause tides are not related to the phenomena which cause storms. Therefore, a storm may occur with any tide that is possible during storm season.

15. Using tidal constituents from NOS analyses of the Boston tide gage, hourly tide heights for the winter season were predicted. The period from 15 October to 30 April was chosen as winter season, and 19 years of this seasonal record were generated to simulate a tidal epoch. Combining the 28 surge time-histories with every possible tide time-history during this tide series would result in more than 2.5 million combinations. Obviously, it would be economically impossible to simulate all these possibilities. Furthermore, it is not necessary to simulate a large percentage of the possibilities in order to adequately represent the population. In order to form a representative sample of the total ensemble, a random selection process was devised.

16. The 28 surge time-histories were combined with a large number of tide time-histories. Each of these synthetic surge plus tide time-histories was created from storm and tide time-histories by randomly choosing a starting point in the tide series, matching this point to the start of a storm, and adding the tide and surge levels at each hour for the length of the storm. The resulting large number of possible event time-histories served as the data set from which events were randomly selected for simulation by the numerical models. Each of the 26 storms, in the 20-year partial duration series of surge, was combined with 500 tide time-histories chosen at random from the 19-year tide series. Each of these storms was considered to have an equal likelihood of occurrence (each storm did, in fact, occur during the 20 years). The two additional storms (1945 and 1978) were not part of the 20-year partial

duration series and, therefore, did not have the same likelihood of occurrence as the other 26 members in the ensemble. Therefore, these two extra storms were combined with a fewer number of tides. To determine the number of events which should be formed using these two storms, the following simplified analysis was used. The 1945 and 1978 storms had the first and second largest surges in a 58-year annual series (the length of available data). Assuming a Weibull plotting position formula, $p = m/N+1$, where m is the rank and $N = 58$, the 1945 and the 1978 surges would have frequencies of 1/59 and 2/59, respectively. Assuming the other 26 members of the storm ensemble to have frequencies of 1/20, and using the ratios of these frequencies, the 1945 storm was combined with 170 tides and the 1978 storm with 340 tides. For example, $(1/59) / (1/20) \times 500 = 170$. This analysis is not rigorous from a statistical standpoint and was done primarily to prevent the two storms with the strongest winds and largest waves from being overrepresented at low and medium water levels. Approximately 13,500 possible surge plus tide time-histories resulted from this process ($26 \times 500 + 340 + 170$). Events to be simulated were selected from this file of possible surge plus tide time-histories.

Selecting Events to Model

17. A flood-causing event is multidimensional. The severity of the damage caused by the event is determined by several factors, among which are the magnitude and duration of winds, waves, and water levels. Because of the difficulty of ranking multidimensional entities, as well as the lack of available data for doing so, it is necessary to reduce the dimensionality. Therefore, only one dimension, maximum still-water level, was used to measure the severity of an event. This criterion was chosen for two main reasons. First, it was deemed the most important; and, second, there was a large volume of available data. NED has established a stage-frequency curve (Figure 4) at (NED 1983) relating maximum still-water level with its frequency of occurrence the Boston NOS tide gage. This stage-frequency curve was used as the basis for both event selection and the assignment of probability to simulated events.

18. Based upon previous experience (Prater, Hardy, and Butler, in preparation) it was estimated that by simulating 50 events the frequency of still-water level would be accurately represented throughout the study area.

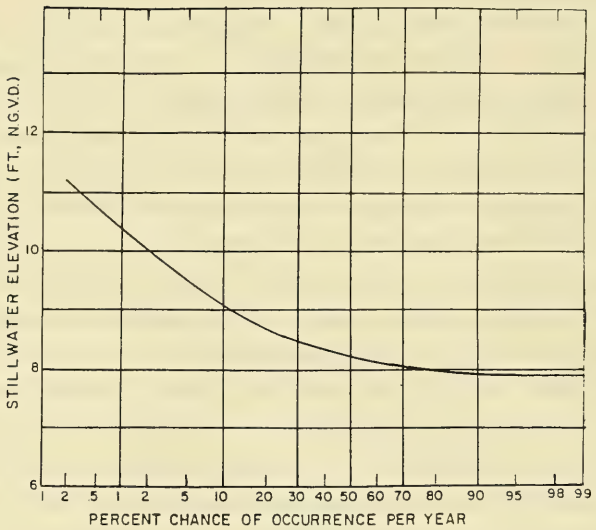

Figure 4. NED stage-frequency curve for Boston

still-water level would be accurately represented throughout the study area. However, the extra variables involved in simulating waves and wave overtopping volumes would cause added uncertainty in the final frequency curves at Roughans Point. Therefore, it was decided to simulate 150 events in order to increase the confidence that the frequency curves based upon overtopping calculations were accurate. The 150 events were selected and simulated, and then frequencies were calculated in three separate sets, each containing 50 events. This was done to establish a measure of confidence in the selection procedure. This confidence calculation will be explained in Part VI.

19. The selection process involved four steps. First, the stage increments, for which simulations were to be performed, were chosen. As previously mentioned, the highest still-water level on record for the Boston area is 10.3 ft NGVD, which occurred during the February 1978 northeaster. As predicted by the NED curve, the 500-year level is 11.2 ft NGVD, and the annual level is 7.9 ft NGVD. Events were selected to duplicate the NED stage-frequency curve below the 500-year level at the Boston gage. Therefore, given the small range in elevation and choosing three sets of 50 events, selections were made every 0.1 ft from 7.9 to 10.4 ft and every 0.2 ft from 10.4 to 11.2 ft. Next, the number of events to be selected at each stage increment

was decided. The results of these first two processes are shown in Table 2. Examining Table 2, it can be seen that more events were selected for the lower range of water levels (≈8 ft NGVD) than were selected for the higher water levels (above 10.5 ft NGVD). This was done for two reasons. First, the probability mass representing the lower part of the NED curve will be much larger than the probability mass representing the higher portion of the curve. This is caused by the logarithmic nature of the frequency of water levels. Experience has shown that frequency curves are more easily constructed when the probability masses assigned to simulated events vary as little as possible. For example, the probability mass per year associated with a 0.1-ft increment located at 8.0 ft on the NED curve is 0.14; whereas, the probability mass per year for a 0.2-ft increment at 11.2 ft is 0.00035. Therefore, more events were selected at the lower return periods to divide this large probability mass into smaller segments. Secondly, especially when considering overtopping, events formed from many more combinations are possible at the lower stages (large surge plus low tide plus medium waves, small surge plus medium tide plus large waves, etc). At the higher stages fewer combinations are possible (large surge plus large tide plus large waves). Consequently, the higher end of the curve can be represented by fewer events than can the lower end.

20. Choosing the stage increment sizes and the number of events selected for simulation from each increment is a subjective decision. This decision is based on the range of stages to be represented, the largest differences in probability tolerable for accurate curve generation, and the financial constraints on the number of events that can be simulated. Unfortunately, the only sure way to determine if the decisions are correct is to view the results. Therefore selections are made, and the goodness of these decisions is reflected in the error bands presented in Part VIII.

21. The third part of the selection process is the actual selection of events. The 13,500 possible events, created by combining the storm surge with tide, were ranked by the maximum water level that occurred during the surge plus tide time-history. At each of the stage increments shown in Table 2, events were randomly selected from the portion of the 13,500 events with maximum water level equal to that height increment. This was done independently for each of the three sets of 50 events. Although these maximum water levels are for the Boston NOS tide gage, events selected for simulation in the study

Center of Height Increment ft, NGVD	Number Selected	Center of Height Increment ft, NGVD	Number Selected
7.9	5	9.4	1
8.0	4	9.5	1
8.1	4	9.6	1
8.2	3	9.7	1
8.3	3	9.8	1
8.4	3	9.9	1
8.5	2	10.0	1
8.6	2	10.1	1
8.7	2	10.2	1
8.8	2	10.3	1
8.9	1	10.4	1
9.0	1	10.6	1
9.1	1	10.8	1
9.2	1	11.0	1
9.3	1	11.2	1

NOTE: These are the numbers of events selected for each set of 50 events. Total events selected at each height increment would be three times the numbers found in this table.

area were chosen from this ranked set. This method of transferring these surge plus tide time-histories to the study area was determined during calibration of the storm surge model (see Part III).

22. Figure 5 shows the fourth and final part of the selection process, the assignment of probability to the selected events. The probability p, represented by each stage increment, is calculated by taking the difference of the exceedance probabilities P of the end points of the increment. If more than one event was selected to represent that stage increment, then the probability assigned to that increment is divided equally among the chosen events. Table 3 contains the maximum water levels (predicted at the Boston gage) and the probabilities assigned to the three sets of selected events. The column in Table 3 labeled "Storm" refers to the numbering of the storms in Table 1. Note that since the selection process is random, not all the storms are represented in each of the three sets of 50 events (denoted as A, B, and C in Table 3), and the number of times a storm is chosen varies from set to set. In conclusion, the essence of the selection process is to choose events for simulation so that the stage-frequency curve, for a known location is

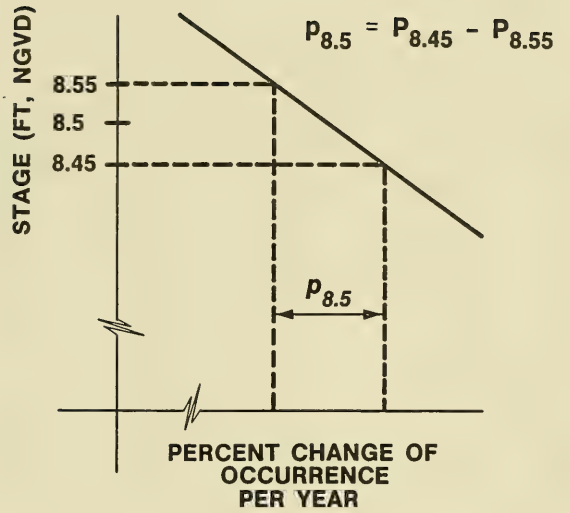

Figure 5. Assigning probabilities to events selected for simulation

duplicated by a limited number of events. When these events are simulated, the probability masses assigned to the events are used to construct stage-frequency curves throughout the modeled area.

Table 3

Events Selected for Modeling

Storm	Set A Max. Level ft, NGVD	Set A Prob.	Set B Max. Level ft, NGVD	Set B Prob.	Set C Max. Level ft, NGVD	Set C Prob.
1	8.3	0.0223	9.9	0.0031	9.3	0.0115
	10.0	0.00375	10.3	0.0018	9.5	0.0093
	10.3	0.0018	10.6	0.0021	10.9	0.00115
	10.4	0.0022	10.7	0.0016	--	--
2	8.0	0.0350	--	--	8.1	0.0250
	8.3	0.0223	--	--	--	--
3	7.9	0.0420	8.1	0.0250	8.3	0.0223
	8.7	0.0160	9.6	0.0082	8.4	0.0183
	9.8	0.0045	10.1	0.0025	8.7	0.0160
	10.1	0.0025	--	--	--	--
4	8.2	0.0293	--	--	7.9	0.0420
5	8.4	0.0183	7.9	0.0420	8.1	0.0250
6	9.4	0.0090	8.1	0.0250	8.0	0.0350
	--	--	8.6	0.0190	8.6	0.0190
	--	--	--	--	9.8	0.0045
7	8.8	0.0145	7.9	0.0420	8.2	0.0293
	9.3	0.0115	--	--	8.3	0.0223
	--	--	--	--	9.7	0.0045
8	--	--	--	--	8.1	0.0250
	--	--	--	--	8.5	0.0250
	--	--	--	--	8.5	0.0250
9	8.1	0.0250	8.2	0.0293	9.6	0.0082
	8.9	0.0220	--	--	--	--
10	7.9	0.0420	8.1	0.0250	8.0	0.0350
	9.2	0.0135	8.4	0.0183	--	--
11	8.4	0.0183	8.8	0.0145	--	--
	8.8	0.0145	--	--	--	--
12	8.0	0.0350	7.9	0.0420	--	--
	8.7	0.0160	8.8	0.0145	--	--
13	8.2	0.0293	9.5	0.0093	8.1	0.0250
	10.2	0.0026	--	--	--	--

(Continued)

Table 3 (Continued)

Storm	Set A Max. Level ft, NGVD	Set A Prob.	Set B Max. Level ft, NGVD	Set B Prob.	Set C Max. Level ft, NGVD	Set C Prob.
14	8.6	0.0190	7.9	0.0420	8.4	0.0183
	8.6	0.0190	--	--	8.6	0.0190
15	8.0	0.0350	8.1	0.0250	--	--
	10.7	0.0016	9.3	0.0115	--	--
	--	--	9.7	0.0045	--	--
16	7.9	0.0420	--	--	--	--
	8.1	0.0250	--	--	--	--
17	--	--	8.4	0.0183	8.8	0.0145
	--	--	--	--	8.9	0.0220
18	--	--	--	--	8.0	0.0350
	--	--	--	--	9.0	0.0190
19	8.3	0.0223	8.2	0.0293	7.9	0.0420
	9.9	0.0031	8.7	0.0160	8.2	0.0293
	--	--	8.9	0.0220	--	--
20	--	--	8.2	0.0293	10.1	0.0025
	--	--	9.1	0.0165	10.5	0.0021
21	8.0	0.0350	8.0	0.0350	--	--
	8.1	0.0250	8.0	0.0350	--	--
	8.5	0.0250	8.7	0.0160	--	--
22	7.9	0.0420	8.6	0.0190	7.9	0.0420
	7.9	0.0420	9.0	0.0190	7.9	0.0420
	--	--	--	--	8.8	0.0145
	--	--	--	--	9.2	0.0135
23	--	--	8.3	0.0223	9.4	0.0090
	--	--	8.3	0.0223	--	--
24	--	--	--	--	8.2	0.0293
	--	--	--	--	8.7	0.0160
25	8.2	0.0293	7.9	0.0420	8.3	0.0223
	8.5	0.0250	10.2	0.0026	10.2	0.0026
	9.0	0.0190	10.4	0.0022	10.3	0.0018
	9.1	0.0165	10.9	0.00115	10.4	0.0022
	9.5	0.0093	--	--	--	--
26	--	--	8.0	0.0350	9.1	0.0165
	--	--	8.4	0.0183	--	--

(Continued)

Table 3 (Concluded)

Storm	Set A Max. Level ft, NGVD	Set A Prob.	Set B Max. Level ft, NGVD	Set B Prob.	Set C Max. Level ft, NGVD	Set C Prob.
27	8.1	0.0250	8.0	0.0350	7.9	0.0420
	8.4	0.0183	8.5	0.0250	8.0	0.0350
	9.7	0.0045	9.8	0.0045	9.9	0.0031
	--	--	--	--	10.0	0.00275
28	9.6	0.0082	8.3	0.0223	8.4	0.0183
	10.5	0.0021	8.4	0.0250	10.7	0.0016
	11.0	0.00035	9.2	0.0135	11.1	0.00035
	11.1	0.00035	9.4	0.0090	--	--
	--	--	10.0	0.00375	--	--
	--	--	11.1	0.00035	--	--

PART III: STORM SURGE PLUS TIDE SIMULATION

23. The WES Implicit Flooding Model (WIFM) was used as the hydrodynamic storm surge model. A detailed description will not be given in this report. The numerical and hydrodynamic features of WIFM are discussed in Butler (1978) and the application of WIFM to coastal studies is demonstrated in numerous reports (including Butler 1983). WIFM solves the vertically integrated, time-dependent, shallow-water wave equations of fluid motion using an alternating direction, implicit, finite-difference algorithm. The model allows subgrid barriers which can be non-overtoppable, overtoppable, or submerged. An important feature of WIFM is the capability for using an exponentially stretched numerical grid which permits a concentration of grid resolution in areas of interest. Also included in the code is the capability to flood or dry individual cells during a simulation.

Grid Development

24. In order to model storm surge, it is usually necessary to extend the computational grid past the edge of the continental shelf and into deep water. Since it also is desirable to have small cell sizes in areas of interest, a very large number of grid cells may be necessary to model a study area using one grid. Consequently, in locations with a wide continental shelf, as in the present study, a two-grid system is usually developed. A global grid with coarse resolution extends throughout the study area and out past the edge of the continental shelf. A nearshore grid which extends only over the immediate study area but with much finer resolution is also developed. A surge plus tide event is first simulated on the global grid. Then, using boundary conditions saved during the global run, the event is simulated on the nearshore grid.

25. The present study does not use this two-grid system. Because of the project's proximity to the NOS tidal gage in Boston Harbor, a method was devised to use the Boston tide gage in place of a global grid. Use of the single grid resulted in considerable savings avoiding both simulation on an outer grid and stage-frequency curve generation at a connection point between two grids. This process involved setting up a single grid (Figure 6) and then calibrating the model to produce correct water levels throughout the study

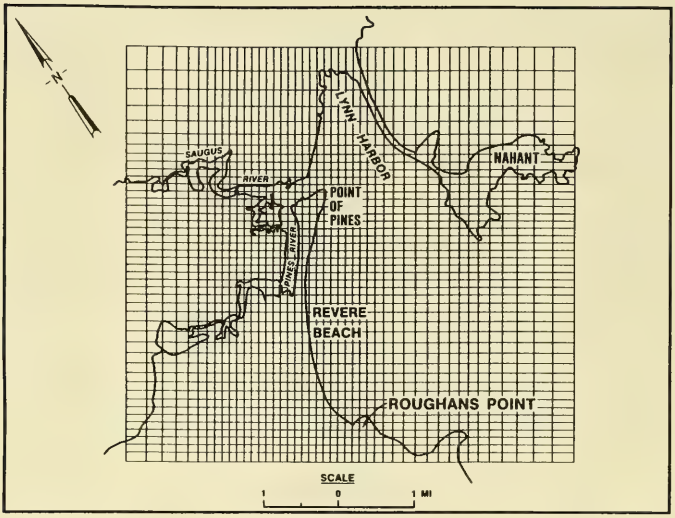

Figure 6. Numerical grid for storm surge model

area using altered Boston water levels to drive the boundary. The procedure used to alter the Boston water levels to produce the desired results is described in the section on model calibration.

26. The final grid configuration has 2,025 cells arranged in 45 rows and 45 columns. The cells with the finest resolution are 500 ft square and cover most of the areas of interest: Roughans Point, Point of Pines, the Saugus-Pines Inlet, and the initial reaches of both rivers. The cells with the coarsest resolution, located near the boundary, are approximately 1,500 by 700 ft. The grid is orientated to match the predominant direction of the river system, since the initial reaches of the rivers form nearly 90-deg angles.

Wind Forcing

27. Wind speed and direction are required inputs to WIFM for the modeling of storm surge. For this study a spatially constant but temporally varying wind forcing was used. The wind data were supplied by NED using raw data from Logan International Airport and a wind data analysis computer program

developed by NED. The wind data were 1-min averages of both wind speed and direction reported hourly and corrected to a 33-ft elevation. The hourly wind data were interpolated to 60-sec time-steps and applied without spatial variation to the entire study area. Two factors allowed this simplified treatment of wind forcing. First, the small geographic area of the modeled area was close to the source of the wind data. Second, the use of Boston tide gage data for boundary conditions already included the effect of the wind over the continental shelf, so the local winds were needed only to locally redistribute the surge. For the 28 northeasters chosen for this study, the average maximum hourly wind speed was 33 knots and varied from 25 knots to 48 knots. The wind directions for these maximum winds varied from 0 to 292 deg (all but three were between 0 and 90 deg) The average direction of the maximum hourly values was 73 deg. Wind directions are referenced clockwise from North.

Data Collection

28. During the summer of 1984, NED supervised the placement and operation of five tide gages in the study area. Figure 7 shows the location of these gages. Two of the gages, Simpson's Pier and Bay Marine Lobster, were located outside the river system at Roughans Point and in Lynn Harbor, respectively. The other three gages (Fox Hill Drawbridge, Broad Sound Tuna, and Atlantic Lobster) are located in the Saugus-Pines River system. All of these gages were in operation from June to October 1984. No other data collection efforts were commissioned solely for numerical modeling. Bathymetric and elevation data for Revere Beach and throughout most of the river system were obtained from previous surveys conducted for beach and channel improvement projects and for highway projects. Excellent data were generally available for the area east of the Salem Turnpike and for the area immediately adjacent to the abandoned highway embankment. Bathymetric data for Lynn Harbor and Broad Sound were obtained from NOS nautical charts.

Model Calibration

29. Since all five study area gages were not operational during any storm and the two gages left in operation during the winter of 1985 did not experience any significant storm induced high water, the model could not be

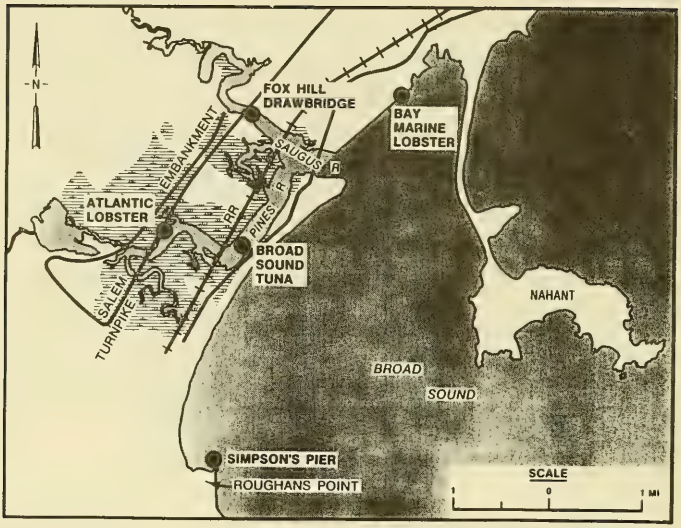

Figure 7. Location of study area tide gages

calibrated or verified to a surge plus tide event. Consequently, two periods during the summer of 1985, one at spring tide and the other at neap tide, were chosen for calibration and verification of the model.

30. A 29-hour period from 0800 29 July to 1300 30 July 1984 was chosen for calibration. During this period data were available from all five study area tide gages, and both the highest tide and the largest range of the month occurred (6.7 and 13.0 ft NGVD, respectively, at Boston). Data from each gage are plotted against data from the NOS gage at Boston (Figures 8-12). The gage at Simpson's Pier went dry at -4.2 ft NGVD resulting in the horizontal lines at low tide in Figure 8. Several facts can be immediately seen from these figures. The range, phase, and MSL of the study area gages are very close to those of the Boston gage. The water levels at high tide are all within several tenths of a foot, and the phases at high tide are all within several minutes. It is interesting that Broad Sound Tuna, a river gage, has the highest tides resulting from a small upward shift in MSL. The largest differences occur at low water where the river gages show a distinctly higher and later low tide, relative to Boston. During the calibration process, adjustments were made in the following items so that the numerical results would

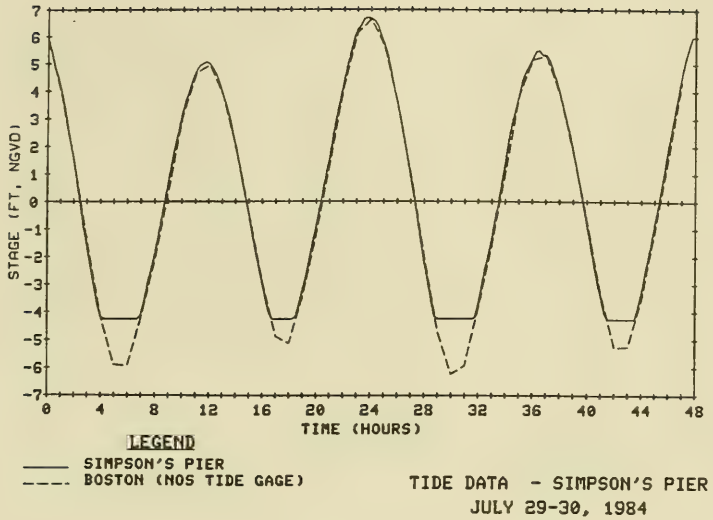

Figure 8. Tidal calibration data, Simpson's Pier

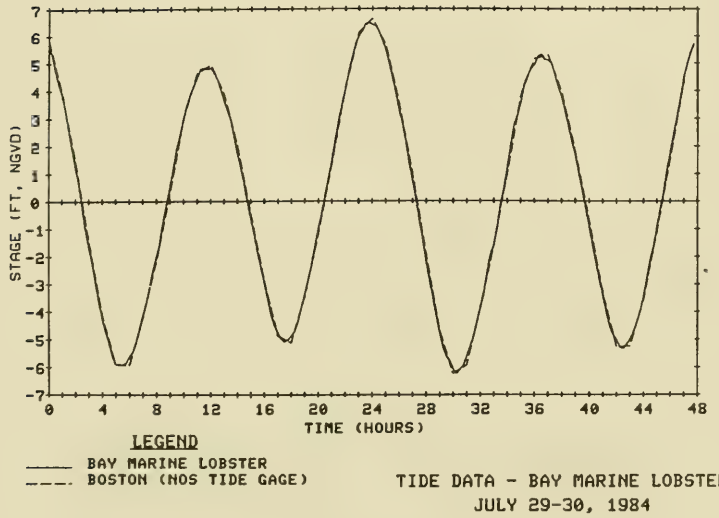

Figure 9. Tidal calibration data, Bay Marine Lobster

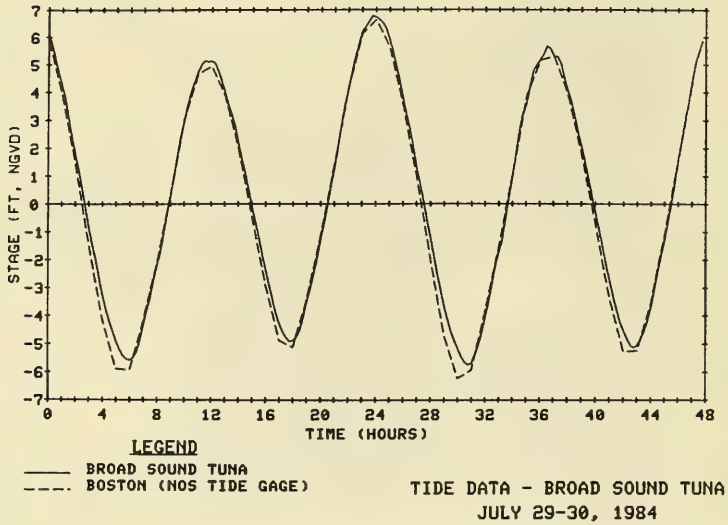

Figure 10. Tidal calibration data, Broad Sound Tuna

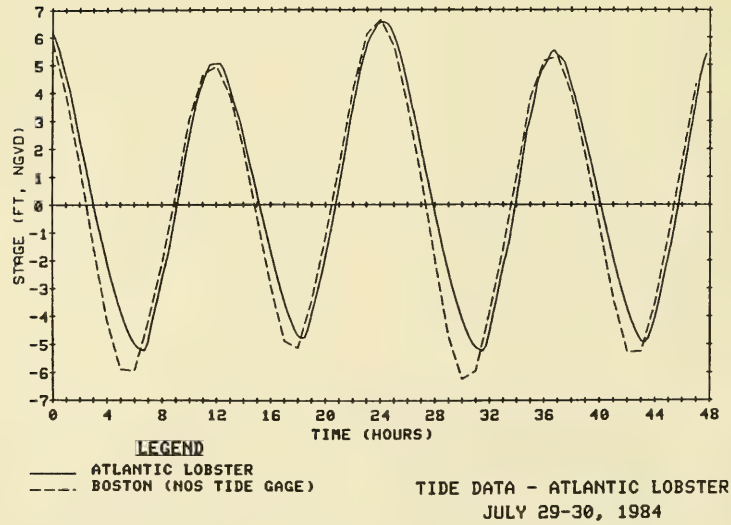

Figure 11. Tidal calibration data, Atlantic Lobster

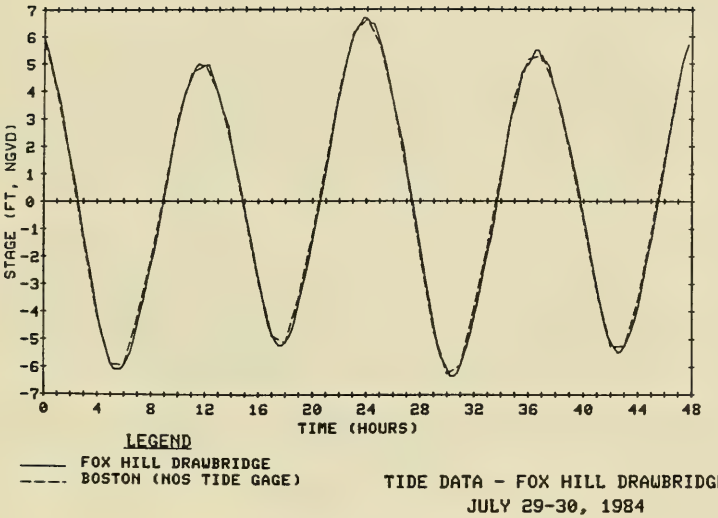

Figure 12. Tidal calibration data, Fox Hill Drawbridge

closely match the tide gage data for the 29-hour period specified above. These adjustments are explained below.

a. Cross-sectional areas and frictional characteristics of both channels and the bridge openings were adjusted. The minimum cell size of 500 ft was much larger than the channel width at many of the constrictions. A smaller cell size would have greatly increased modeling costs; therefore, using the 500-ft cell size necessitated that the flow be adjusted through these oversized areas by alterations in depth and friction. It would have been convenient if the depth could have been adjusted on the oversized cells so that cross-sectional areas would match between model and prototype. However, due to the large tidal range in the study area, matching cross-sectional areas would have caused the channels to dry up well above low water. Consequently, it was necessary to make these cells deeper than the area represented in the prototype would justify. Higher water levels would cause excessive flow through these oversized channels. A compromise depth was selected so that the channel would remain flowing at low water levels. At low water the opposite problem would occur. Since the depth of the channels in the study area is much greater than the compromise depth used in the model cells, the flow restriction is higher in the model than in the prototype. This causes a reduction in flow in the model at low water. Therefore, in addition to the compromise depth, frictional characteristics were made dependent upon depth to produce smaller Manning's n values at low

water and greater n values at higher water. With these adjustments, the model was able to duplicate the calibration data in the Saugus-Pines river system.

b. Storage in both channel and ponds in upper reaches of both rivers was adjusted in order to match elevations, particularly those measured at Atlantic Lobster and Broad Sound Tuna. Very little bathymetric data and no tidal data were available for these areas. Therefore, storage was at first estimated from USGS topographic maps and then changed during the calibration process. The final storage areas selected remained reasonable based upon the available data.

c. As was mentioned previously, data from the Boston gage were adapted for use as boundary conditions for the model. Since the tide in the study area conforms so closely with that measured at Boston, only minor alterations to the Boston tide were necessary. The calibration process found that Boston data should be multiplied by 0.984 and shifted forward in time by 5 min before being used as boundary values.

31. The results of the calibration process are depicted in Figures 13-17. These figures show excellent agreement between numerical and measured water levels during a period of large tidal range.

Model Verification

32. A 32-hour period from 1000 15 August to 1800 16 August 1984 was chosen to verify the hydrodynamic model. This time period was chosen because good data were available from the five study area tide gages as well as from the NOS gage at Boston. Also, since the calibration was preformed for a spring tide, a neap tide with a lower high tide and a small range (4.8 and 8.2 ft NGVD, respectively) was chosen to verify the model. The results for the five study area gages are shown in Figures 18-22. These results show excellent agreement between numerical and measured water levels for all five locations.

Simulation of Event Ensemble by the Hydrodynamic Model

33. The 150 selected events were simulated on a CYBER 205 computer in three sets of 50 by the calibrated and verified storm surge model. The simulations of the individual events varied from 13 to 75 hours prototype time depending upon the number of high tides that needed to be modeled. For each of the 150 surge plus tide time-histories, all highs with still-water levels

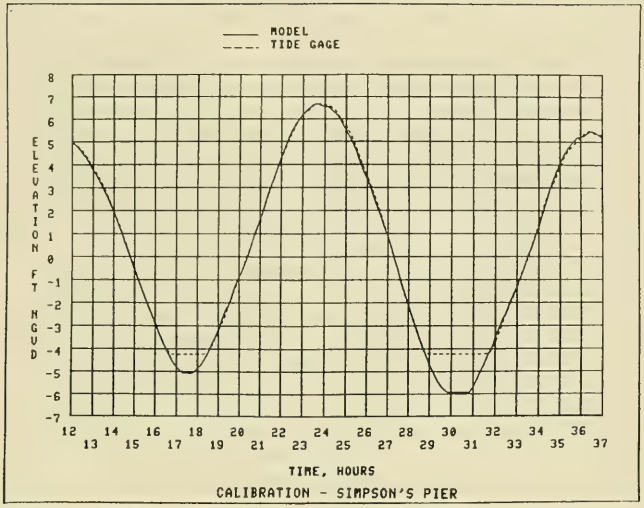

Figure 13. Surge model calibration results, Simpson's Pier

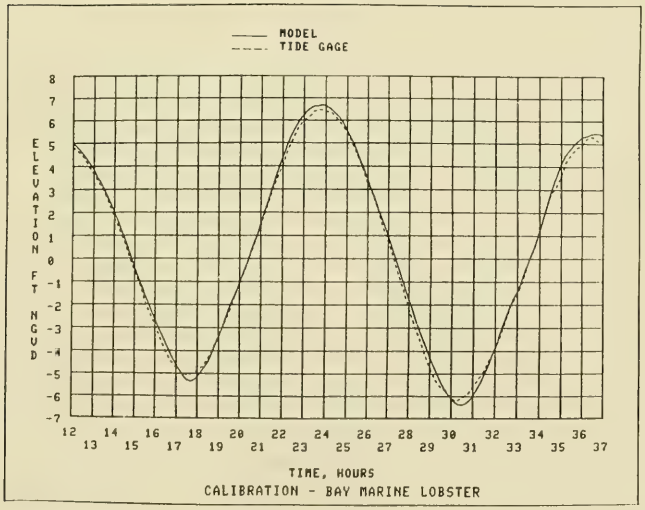

Figure 14. Surge model calibration results, Bay Marine Lobster

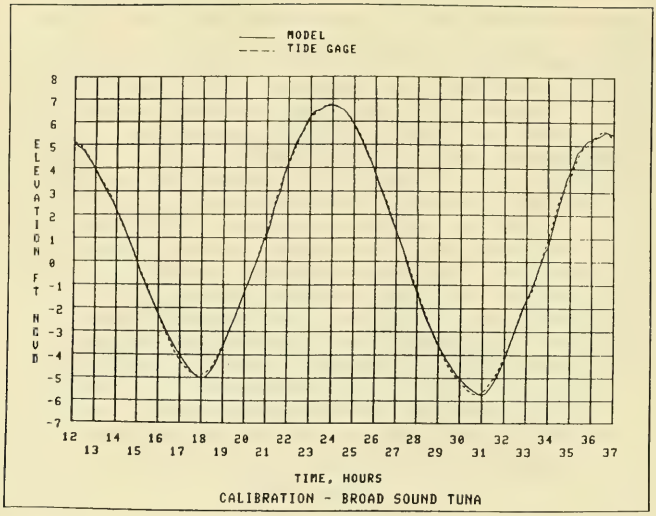

Figure 15. Surge model calibration results, Broad Sound Tuna

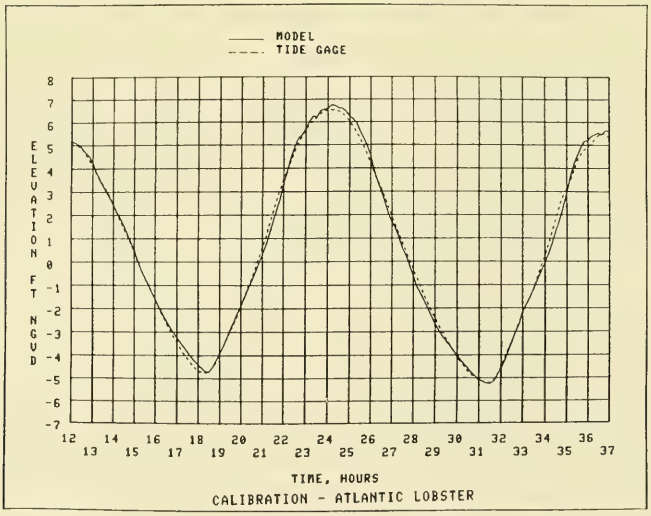

Figure 16. Surge model calibration results, Atlantic Lobster

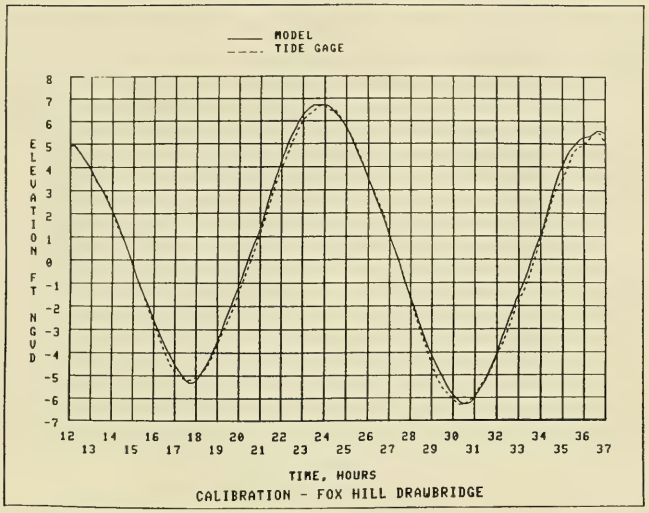

Figure 17. Surge model calibration results, Fox Hill Drawbridge

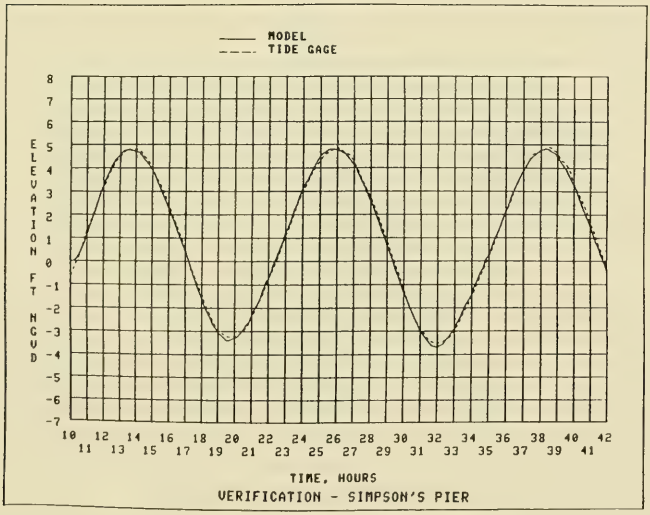

Figure 18. Surge model verification results, Simpson's Pier

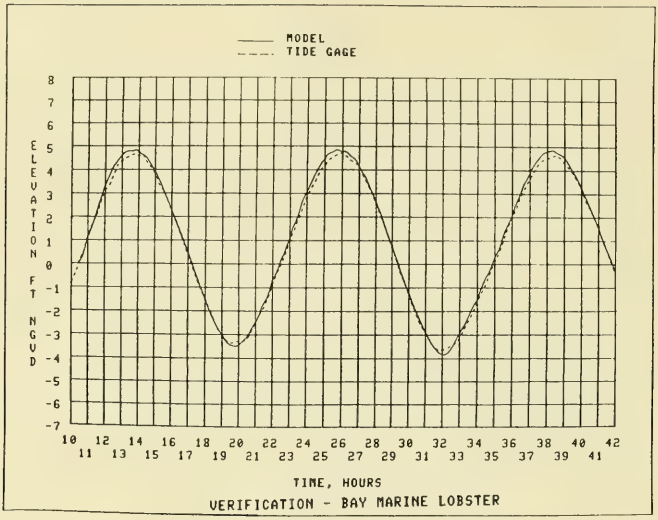

Figure 19. Surge model verification results, Bay Marine Lobster

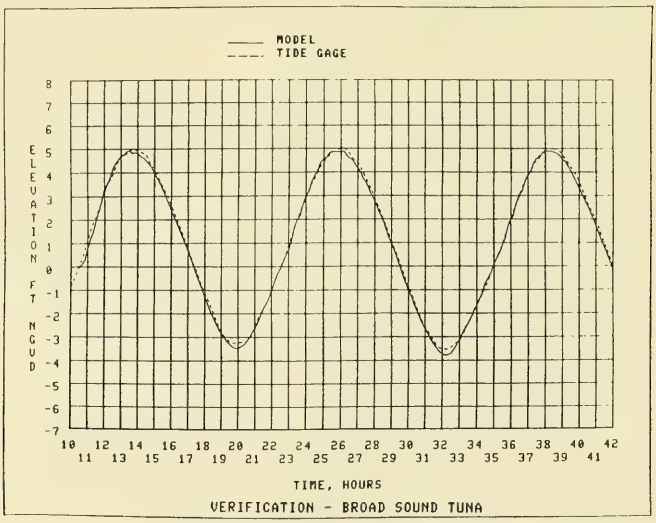

Figure 20. Surge model verification results, Broad Sound Tuna

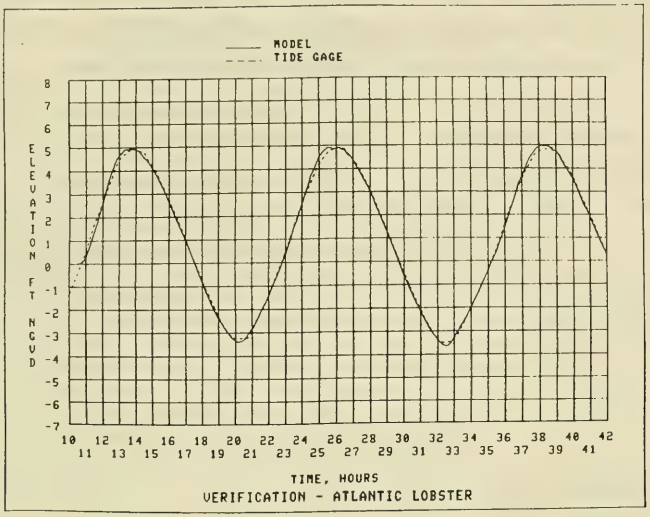

Figure 21. Surge model verification results, Atlantic Lobster

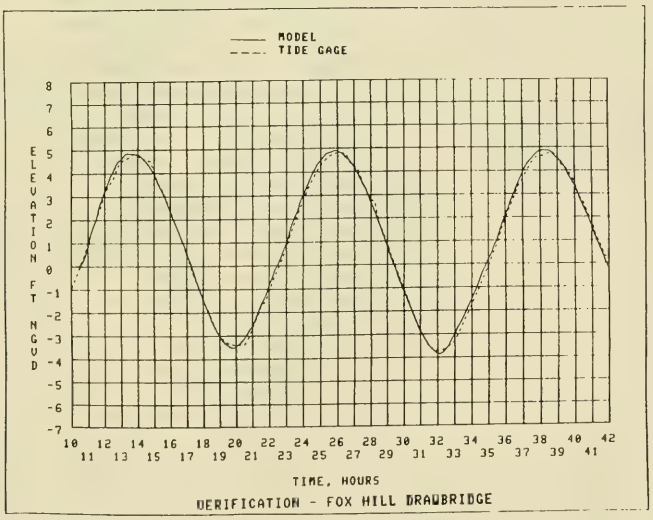

Figure 22. Surge model verification results, Fox Hill Drawbridge

greater than 7.0 ft NGVD were included in the simulation. A constant time-step of 60 sec was used for all events. Two computer files, saving information at each of the numerical gage locations shown in Figure 23, were the main result of each simulation. The first file was a time-history of water levels at 15-min increments. This file was used both to plot the water level time-histories at each numerical gage and to provide information to the computer codes which calculated wave overtopping rates and interior volumes at Roughans Point. The second file listed the maximum elevation experienced at each of the numerical gages during each event. This file was used to construct the stage-frequency curves for the still-water locations. Both of these computer files were given to NED on magnetic tape.

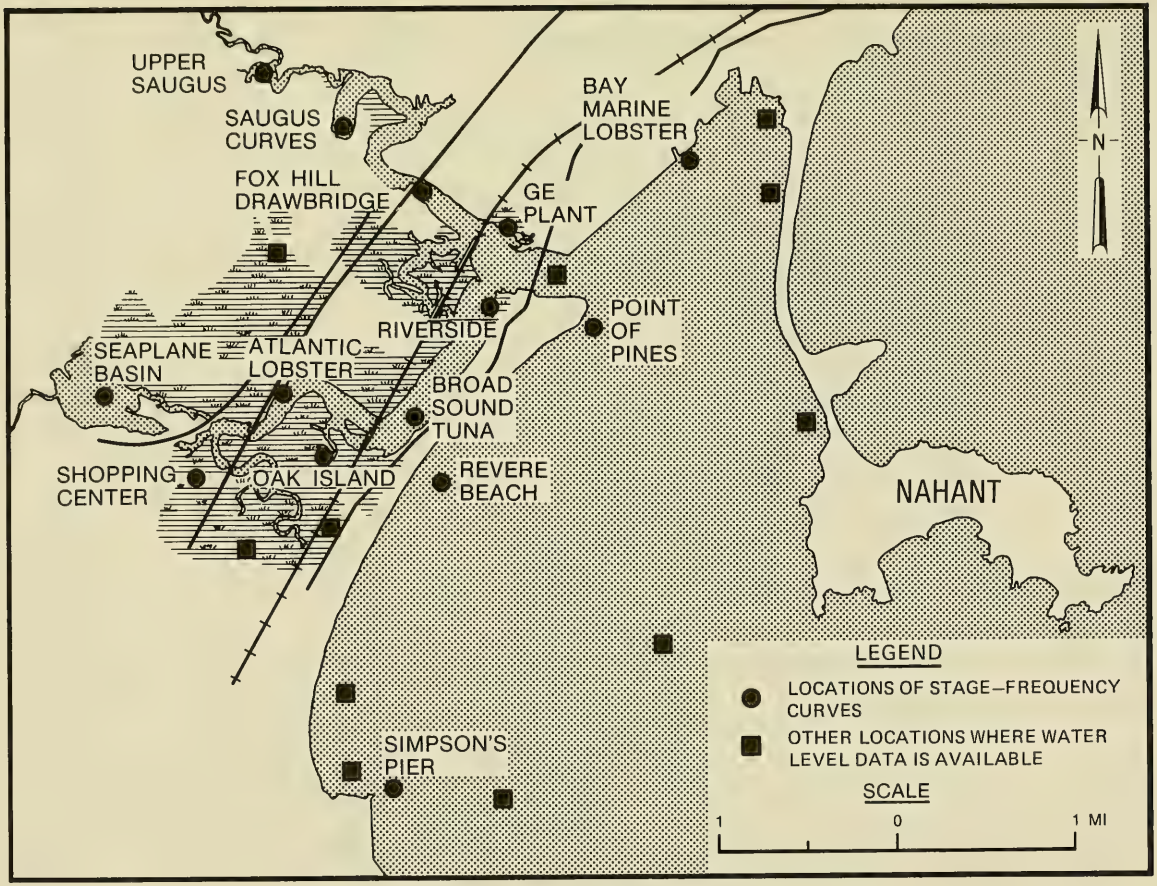

Figure 23. Location of surge model numerical gages

34. For each event (surge plus tide), the wave climate in a 25.9-square mile area of Broad Sound was simulated for each hour when the still-water level was above 7.0 ft NGVD. The area considered is shown in Figure 24. Depths, at mean low water, range from 0 ft at the beaches to approximately 82 ft along the eastern boundary of the grid. The shallow depths in the area required the use of a shallow-water wave model.

35. A steady-state, shallow-water, directional-spectral wave model (ESCUBED) was used to perform the simulations. The required simulations actually called for the use of a time-dependent model, but the cost of using such a model was prohibitive. In lieu of a truly transient simulation, ESCUBED was run once for each hour of each event, and the resulting wave climate was taken to be representative of the conditions existing for the entire hour.

36. For each run of ESCUBED it was necessary to specify a directional spectrum at points along the eastern boundary of the grid shown in Figure 24. To do this, wave train characteristics (e.g. significant wave heights and peak spectral wave periods) were used to define the TMA spectral shape (Hughes 1984), and the resulting one-dimensional spectrum was then distributed directionally. The wave train characteristics represented both sea and swell and were derived using the methods and data of WIS.

37. A total of 848 hr of simulation was made. Resulting wave heights in the lee of Nahant peninsula indicated that local wave generation in this area was inadequately simulated by ESCUBED. Hence, an additional analysis was required when winds were from the northeast.

38. Shallow-water wave growth equations were used to estimate locally generated wave heights and periods off the north seawall at Roughans Point as well as at Point of Pines and in Lynn Harbor. The total wave climate in these regions was then assumed to be a combination of these locally generated waves and the ESCUBED results.

39. It is important to note that no wave data from Broad Sound were available. Hence, it was not possible to calibrate ESCUBED or to verify its results.

40. The following sections discuss the WIS methods and data, the ESCUBED wave model, and the analysis of local wave generation in the lee of Nahant Peninsula.

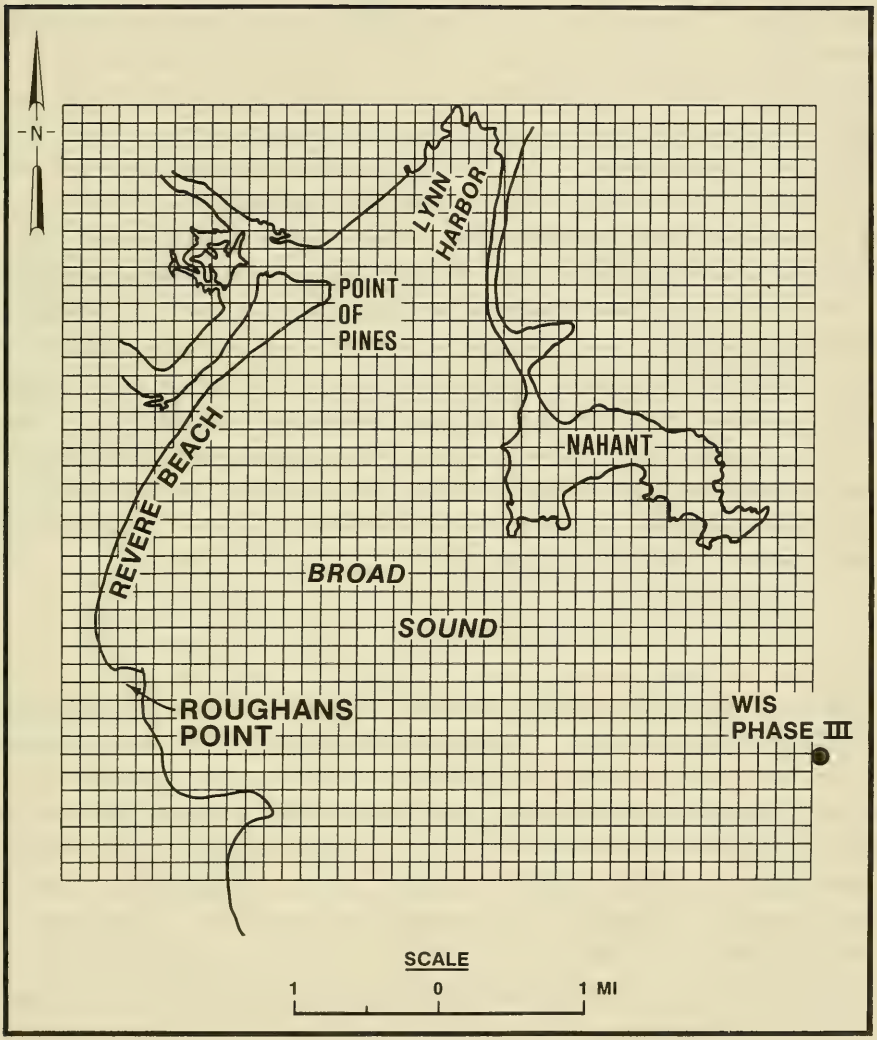

Figure 24. Numerical grid for spectral wave model

WIS Methods and Data

41. In late 1976 a study to produce a wave climate for US coastal waters was initiated at WES. This ongoing study, WIS, consists of three phases. Phase I (Corson et al. 1981) and Phase II (Corson et al. 1982) wave characteristics were generated by a numerical model which simultaneously propagated and transformed the waves over a discrete grid representing segments of the Atlantic Ocean. Phase I acted in the deep ocean. Phase II acted over the continental shelf where, for the purpose of classifying waves, depths may be either intermediate or deep. Phase III draws upon the Phase II data to provide nearshore wave characteristics in depths as shallow as 30 ft. For all three phases, data are available at selected points referred to as stations.

42. WIS methods and data were to be used to establish the boundary conditions for ESCUBED. Theoretically, the ESCUBED grid could have been extended seaward as far as the nearest Phase II station (Phase II stations are approximately 34 miles offshore and 34 miles apart), and the data available at this station could then have been used in the boundary conditions. The costs of computing over such a large grid would have been prohibitive. The Phase III methodology provided an inexpensive bridge between the Phase II station and the much smaller grid actually used.

Phase III Methodology

43. The reader is referred to Jensen (1983) for a complete description of the Phase III methodology. A summary is given here. The Phase II results comprise directional spectra. The Phase III methodology first takes these spectra and separates them into two wave trains, swell and sea. The two are assumed to behave independently. The swell is characterized by the height H, frequency f, and propagation direction θ of a unidirectional, monochromatic wave. The energy of the sea will be distributed in frequency-direction space. A one-dimensional spectrum $E_1(f)$ can be defined in terms of the directional or two-dimensional spectrum $E_2(f,\theta)$ which is expressed as

$$E_1(f) = \int_0^{2\pi} E_2(f,\theta)\, d\theta \qquad (1)$$

44. The Phase III methodology assumes that, at the Phase II station, $E_1(f)$ can be represented parametrically using only two parameters: the energy based significant wave height H_{m_o} and the frequency of the spectral peak f_m. This one-dimensional spectrum is then given a directional distribution using the following equation:

$$E_2(f,\theta) = E_1(f) \frac{8}{3\pi} \cos^4 (\theta - \theta_m) \qquad (2)$$

Here, θ_m is the central angle of the spectrum. $E_2(f,\theta)$ is discretized so that each component can be propagated from the Phase II station to the Phase III station in accordance with linear wave theory.

45. The Phase III methodology assumes straight and parallel bottom contours so that refraction and shoaling of swell and of the discrete elements of $E_2(f,\theta)$ may be determined analytically. The sea is further transformed by wave-wave interactions. Depth-controlled criteria limit both H and H_{m_o}. Sheltering by capes or peninsulas is included in the Phase III methodology.

46. Refraction, shoaling, and depth limitation acting on the swell transform H, f, and θ at the Phase II station into new values in shallow water at the Phase III station. If the Phase III station were sheltered from the swell, then H is zero. Refraction, shoaling, wave-wave interactions, and sheltering acting on individual components of the sea result in a new spectrum for sea at the Phase III station. H_{m_o}, f_m, and θ_m are extracted from this spectrum.

47. The final Phase III result comprises six wave characteristics: H, f, and θ of the swell and H_{m_o}, f_m, and θ_m of the sea. The wave climate at the Phase III station is taken to be completely defined by these six parameters.

Use of Phase III Methodology for Broad Sound Wave Climate Simulations

48. WIS Phase II, sta 13, directional spectra were used as deepwater input. This station is located at latitude 42° 32.5' N and longitude 70° 14' W. The Phase III station was positioned at latitude 42° 23.5' N and longitude

70° 53.5' W (Figure 24). This puts the Phase III station approximately 4.6 mi due east of Roughans Point in 75 ft of water. Cape Ann, to the northeast, and Cape Cod, to the southeast, provided some shelter for the Phase III station. The sheltering was such that only those waves approaching from between N40° E and S60° E could reach the Phase III station.

49. Phase III results were produced at 3-hour intervals. Linear interpolation was used to calculate H , f , θ , H_{m_o} , f_m , and θ_m for every hour.

Wave Climate Simulations for Broad Sound

Summary of ESCUBED

50. The reader is referred to Hubertz (1985) for a detailed discussion of ESCUBED. Relevant aspects of the model are presented here.

51. Essentially, ESCUBED propagates components of discrete directional spectra over a user specified bathymetry. Calculations proceed to propagate individual components of these spectra across a rectangular, uniformly spaced finite difference grid.

52. The grid used for the wave climate simulations at Broad Sound is shown in Figure 24. The grid spacing in both the x and y directions is 656 ft (200 m). At each grid point, the energy of the individual components of a spectrum is limited by the finite depth water equilibrium range proposed by Kitaigorodskii, Krasitskii, and Zaslavakii (1975). The range, which applies for frequencies greater than the peak, is a function of depth and frequency. This limitation could be thought of as an energy sink where the energy loss is through turbulent and viscous processes associated with white capping and large scale breaking.

Determination of a spectrum for the ESCUBED boundary condition

53. The Phase III wave characteristics for sea, H_{m_o} , and f_m were used to generate a TMA spectrum $E_{TMA}(f,h)$ (Hughes 1984). The TMA spectrum is representative of fully developed wind seas in finite depth water.

54. The TMA spectrum was evaluated using the depth at the Phase III station, i.e. $h = 75$ ft . Let $E_{TMA}(f,75\text{ ft}) = E_{TMA}(f)$. The one-dimensional spectrum $E_{TMA}(f)$ was distributed directionally using a $\cos^4(\theta - \theta_m)$ spreading. No energy was allowed to have a direction outside

the WIS Phase III sheltering angles. The total energy of the one-dimensional and directional spectra must be equal. This requirement is expressed as

$$\int_0^{\infty} E_{TMA}(f)df = \int_0^{\infty} \int_0^{2\pi} E_{sea}(f,\theta)\, d\theta\, df \tag{3}$$

where $E_{sea}(f,\theta)$ is the directional spectrum of the sea along the eastern boundary of the ESCUBED grid.

55. Assuming the relationship shown in Equation 4, Equation 5 can be derived from Equation 3. The κ in Equation 5 is a constant which is determined by Equation 6. The limits of integration in Equation 6 match the Phase II sheltering angles since the energy density outside these angles is zero, as indicated below.

$$E_{sea}(f,\theta) = \kappa \cos^4 (\theta - \theta_m)\, E_{TMA}(f) \tag{4}$$

$$\int_0^{\infty} E_{TMA}(f)\, df = \int_0^{2\pi} \kappa \cos^4 (\theta - \theta_m)\, d\theta \int_0^{\infty} E_{TMA}(f)\, df \tag{5}$$

$$\kappa = \left[\int_{(-1/6)\pi}^{(5/18)\pi} \cos^4 (\theta - \theta_m)\, d\theta \right]^{-1} \tag{6}$$

The continuous spectrum, $E_{sea}(f,\theta)$ is discretized using a frequency increment $\Delta f = 0.01$ Hz and a direction increment $\Delta\theta = 20$ deg . Let $E_{sea}(f_i,\theta_i)$ be this discrete spectrum.

56. The final step in determining a directional spectrum representing both sea and swell for the boundary condition at the eastern side of the grid is to add the swell to $E_{sea}(f_i,\theta_i)$. The swell can also be represented by a discrete spectrum, $E_{swell}(f_i,\theta_i)$. If the energy of the swell is uniformly distributed over one frequency-direction band of the spectrum, then a discrete directional spectrum $E_{swell}(f_i,\theta_i)$ can be written as follows:

$$E_{swell}(f_i,\theta_i) = \begin{cases} \frac{H^2}{8\Delta f \Delta\theta} & \text{and} \quad f_i - \frac{1}{2}\Delta f \leq f < f_i + \frac{1}{2}\Delta f \\ & \quad \theta_i - \frac{1}{2}\Delta\theta \leq \theta < \theta_i + \frac{1}{2}\Delta\theta \\ 0 & \text{otherwise} \end{cases} \tag{7}$$

Finally, the discrete directional spectrum used as a boundary condition for ESCUBED is the sum of $E_{sea}(f_i,\theta_i)$ and $E_{swell}(f_i,\theta_i)$.

ESCUBED Results

57. ESCUBED output contains the following information from the wave climate simulations:

a. H_{m_o}, f_m, and θ_m representing the energy based significant wave height, the frequency of the spectral peak, and the direction of the spectral peak at each grid point, respectively.

b. Directional and one-dimensional spectra at selected points in the vicinity of Roughans Point and at points 1.24 miles due east of Roughans Point.

Model results in the lee of Nahant Peninsula indicated that, in this area, ESCUBED inadequately simulated the local wave generation by wind. Although ESCUBED allowed wind energy to be added to the energy of existing waves, ESCUBED did not allow initial growth of waves in the areas sheltered from the WIS input on the boundary. Since these locally generated waves are especially important for waves at the north wall of Roughans Point and for locations along the shore of Broad Sound from Point of Pines into Lynn Harbor, further analysis was required.

Locally Generated Waves in the Lee of Nahant Peninsula

58. The equations for shallow-water wave growth for fetch-limited waves, presented in the Shore Protection Manual (SPM 1984, p. 3-55), were used to obtain an improved determination of the waves attacking the north wall at Roughans Point, at Point of Pines, and at locations in Lynn Harbor.

59. The depth and fetch vary across Broad Sound. At each point where the locally generated analysis was required (see Figure 25 for locations marked A-E), the area was divided into sectors as shown in Figure 26 for the

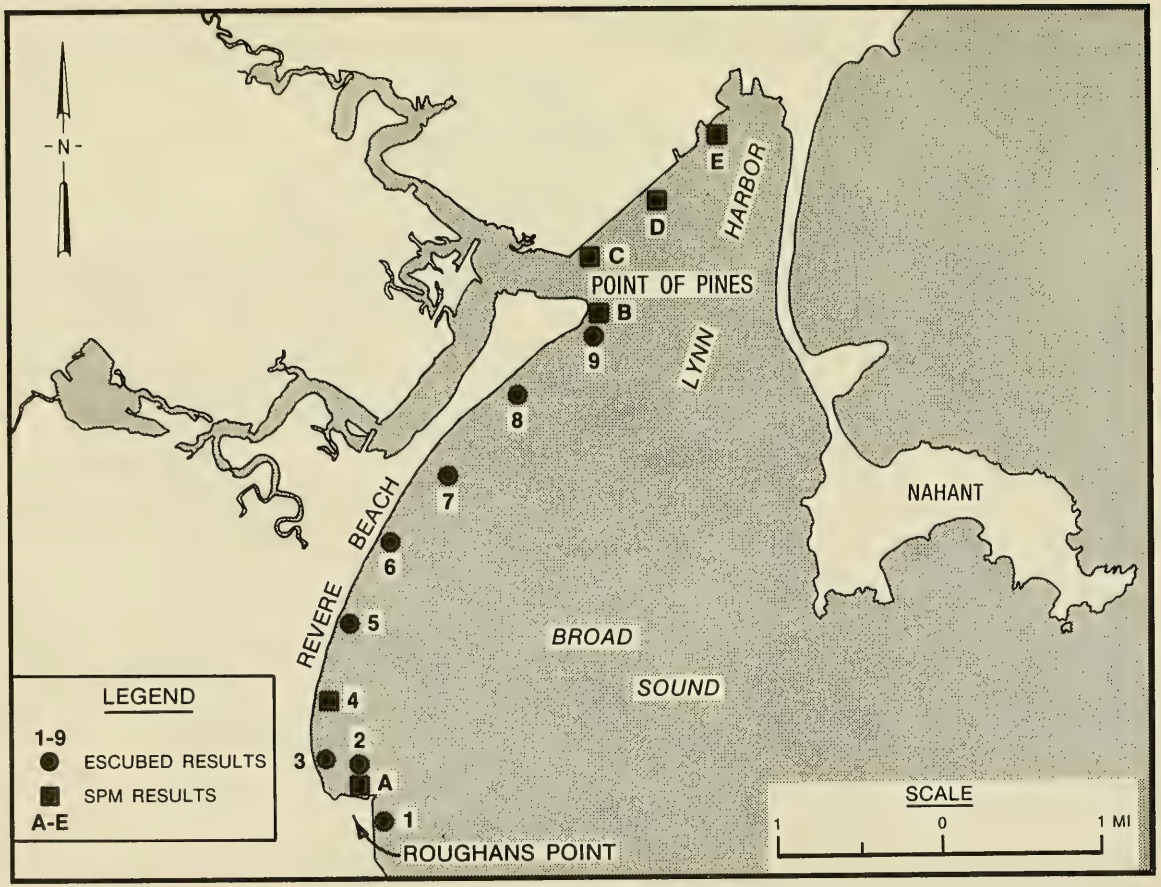

Figure 25. Locations for which locally generated waves were calculated

Roughans Point north wall. A representative fetch and depth were assigned to each sector. For each hour of simulation the appropriate fetch and depth were chosen according to the wind direction. Wave propagation direction was assumed to be the same as wind direction. The sectors, fetch lengths, and depths for the five locations are listed in Table 4. Note that the depth at mean low water (MLW) is listed, but the depth used for the calculations varies with surge and tide. The most important distinction between the ESCUBED and locally generated waves at the Roughans Point north wall is that the ESCUBED

Table 4

Sectors, Fetch Length, and Depths Used for Local Wave Generation

Location	Sector Deg Azimuth		Fetch Length ft	Depth ft, MLW
A	0	25	3,750	2.5
	25	52	5,200	8.0
	52	73	5250	12.0
B	0	34	2,700	7.0
	34	75	6,800	1.0
	65	100	5,600	1.0
	100	117	6,100	1.0
	117	144	8,000	1.0
	144	185	29,600	5.0
	185	216	15,000	1.0
C	51	119	5,300	1.0
	119	131	6,300	1.0
	131	153	8,400	1.0
	153	186	32,000	1.0
	186	231	2,700	7.0
D	51	133	4,300	1.0
	133	145	5,400	1.0
	145	161	9,700	1.0
	161	187	32,800	5.0
	187	205	20,500	5.0
	205	231	3,700	7.0
E	51	95	3,000	20.0
	95	123	3,100	1.0
	123	153	3,600	1.0
	153	167	9,800	1.0
	167	188	33,600	5.0
	188	213	21,300	5.0
	213	231	4,900	7.0

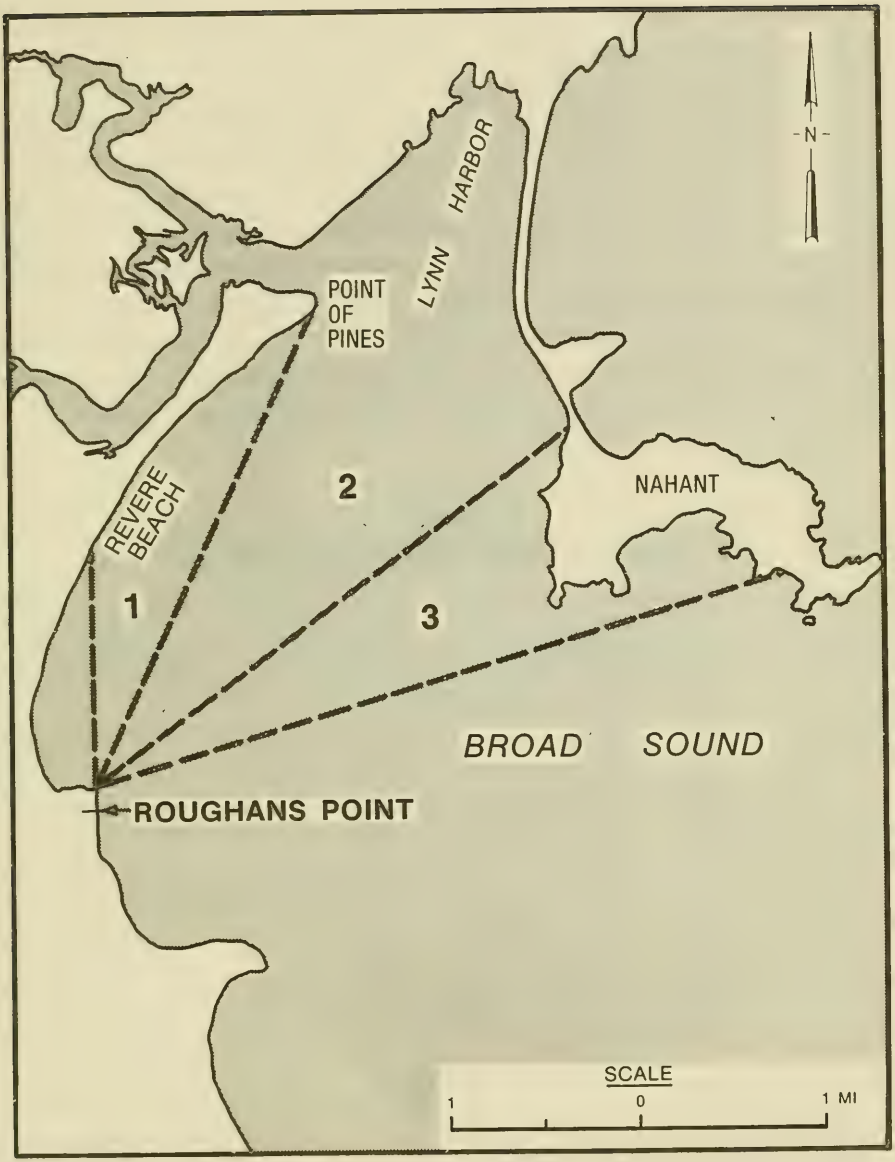

Figure 26. Three sectors used for determining locally generated waves at Roughans Point North Wall

waves attack the wall at oblique angles, whereas the locally generated waves have a more perpendicular angle of attack. For the Lynn Harbor locations the ESCUBED results are essentially negligible, and therefore, the locally generated waves dominate for these locations.

60. Table 5 is a summary of the wave heights, periods, and directions from the ESCUBED modeling for several locations from Roughans Point up along Revere Beach to Point of Pines. These locations are marked 1-9 in Figure 25. Table 6 is a summary of the locally generated waves. These areas are marked A-E in Figure 25. These two tables are provided to demonstrate the range of wave parameters generated by the models. Waves were modeled only during periods of possible overtopping at Roughans Point (water levels above 7.0 ft NGVD) during northeaster conditions. The average values shown do not take into account the varying probabilities of the surge-tide-wave events.

Table 5

Summary of ESCUBED Wave Parameter Results

	Height, ft			Period, sec			Direction, deg True N		
Location*	Min.	Avg.	Max.	Min.	Avg.	Max.	Min.	Avg.	Max.
1	0.5	5.9	9.6	1.9	9.3	14.3	30	92	97
2	0.2	1.9	3.4	1.7	7.9	14.3	**	**	**
3	0.4	5.4	9.5	1.9	8.9	14.3	31	91	103
4	0.2	3.9	8.7	1.7	9.1	14.3	34	109	111
5	0.2	5.1	9.6	2.0	9.1	14.3	100	114	149
6	0.2	4.5	9.1	2.0	9.1	14.3	100	122	149
7	0.2	3.4	8.0	2.0	9.1	14.3	100	130	149
8	0.2	1.8	4.3	2.0	9.1	14.3	100	145	149
9	0.2	0.2	0.3	1.9	3.8	4.3	100	141	150

* Refer to Figure 25 for locations.

** Wave height for the north wall was calculated from the two direction bands (70 and 50 deg) which were the closest to normal to the north wall. No direction was calculated for these waves.

Table 6

Summary of Locally Generated Wave Results

Location*	Height, ft			Period, sec			Direction, deg True N		
	Min.	Avg.	Max.	Min.	Avg.	Max.	Min.	Avg.	Max.
A	0.3	1.8	3.7	1.2	2.3	3.3	0.0	31.4	67.5
B	0.1	1.1	2.4	0.6	1.6	2.9	0.0	41.0	202.5
C	0.4	1.3	2.4	1.2	1.9	3.0	67.5	84.3	225.0
D	0.3	1.2	2.4	1.1	1.8	3.0	67.5	84.6	225.0
E	0.3	1.0	2.4	1.0	1.6	3.0	67.5	84.3	225.0

* Refer to Figure 25 for location.

PART V: FLOOD STAGES FOR THE INTERIOR OF ROUGHANS POINT

61. Once water levels, waves, and probabilities were determined for the simulated events, three processes remained before stage-frequency curves for the interior of Roughans Point could be constructed. These processes were the physical modeling of both existing and proposed Roughans Point structures, calculation of the overtopping rates, and routing of the resulting volumes through the Roughans Point area.

62. A two-dimensional physical model study was conducted to determine a method to calculate the overtopping rates at Roughans Point. Figure 27 is a map of Roughans Point showing the four northern reaches (A, B, C, and D) and the two eastern reaches (E and F). Reach B was not included in the overtopping analysis because its angle of orientation does not allow for direct wave attack. Reach F was not included in the overtopping analysis since water coming over this reach should flow toward the south away from Roughans Point. The structure chosen for reach E will be continued for reach F, both to provide protection for the integrity of the existing wall at reach F and to provide a more suitable termination location for the structure. Model tests were run for one proposed northern structure, the existing eastern structure, and five alternative eastern structures. Analysis of the existing northern structures (A, C, and D) was accomplished using overtopping data from a previous model study. Figures 28-31 contain drawings of the existing and originally proposed structure cross sections (NED 1983). Additional physical model tests, varying the shape of the revetment and the height of the wall, were conducted for the alternative structures for reach E (Figure 32). Only one proposed northern structure was tested, and it was used at all the north reach locations during simulations of the five different reach E alternatives. The pertinent facts for the 10 structures are included in Table 7. For complete details of the physical modeling see Ahrens and Heimbaugh (in preparation).

63. The results of the physical modeling were coefficients (Q_0 and C_1 in Table 6) for an overtopping rate equation (Equation 8). As indicated below, Equation 8 determines overtopping rate per foot of structure length with structure height, water level, wave height, and wave length as the independent variables.

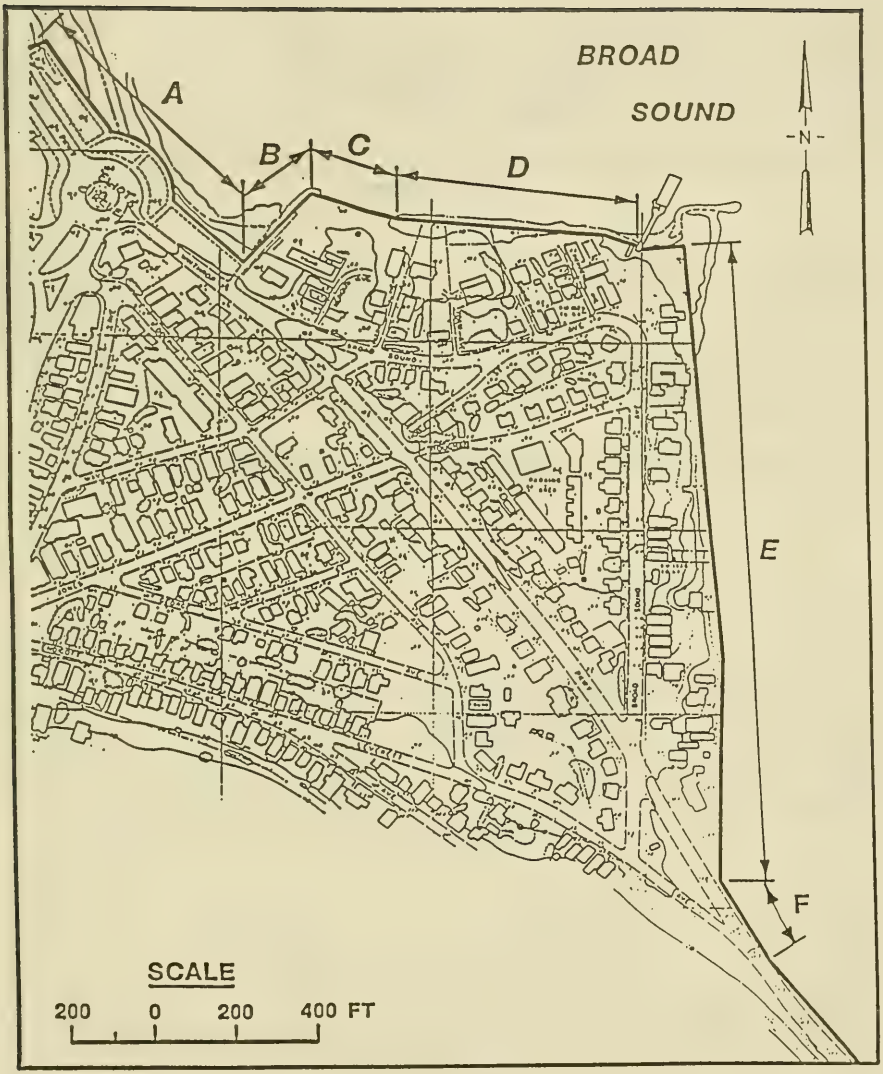

Figure 27. Location of reaches A-F at Roughans Point

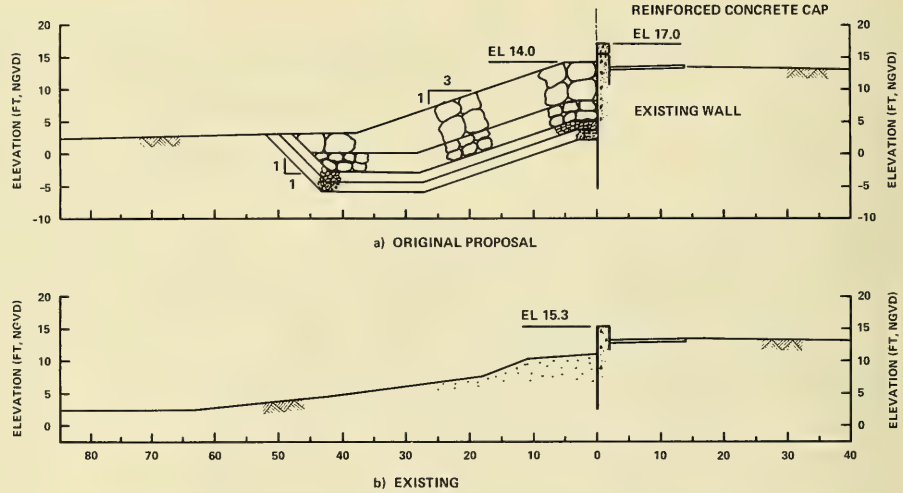

Figure 28. Existing and originally proposed Roughans Point structures for reach A

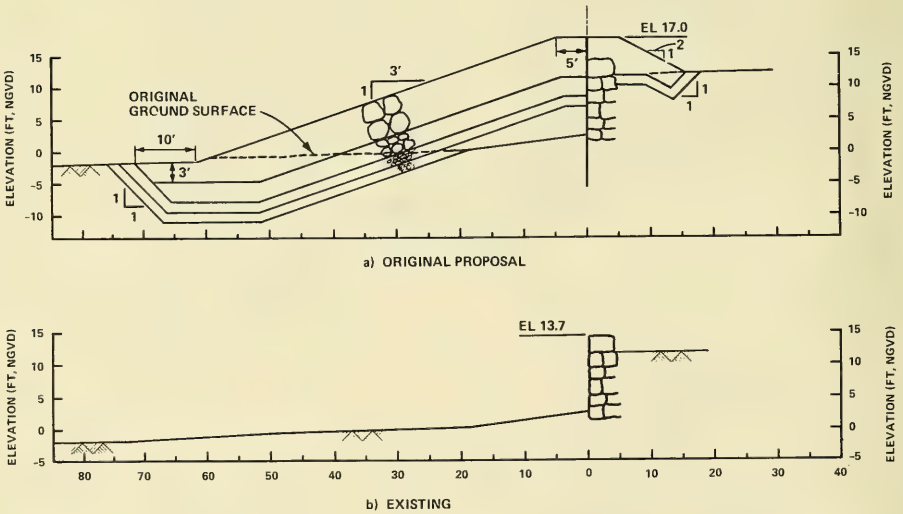

Figure 29. Existing and originally proposed Roughans Point structures for reach C

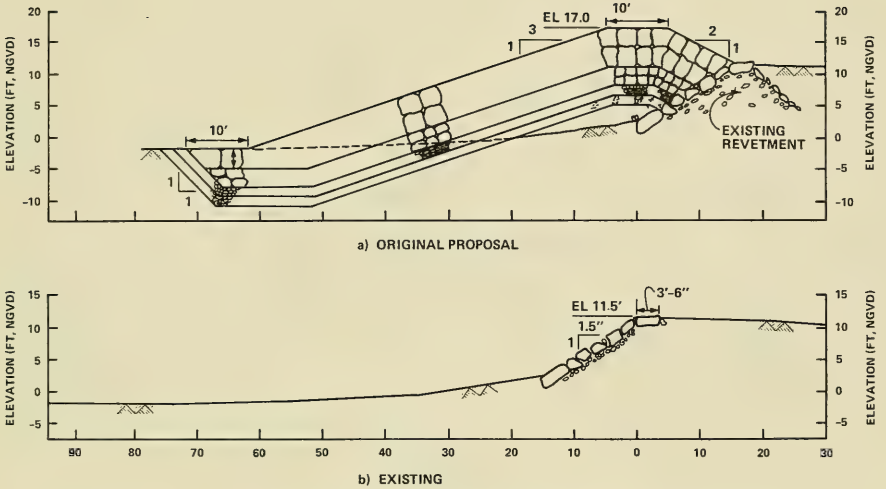

Figure 30. Existing and originally proposed Roughans Point structures for reach D

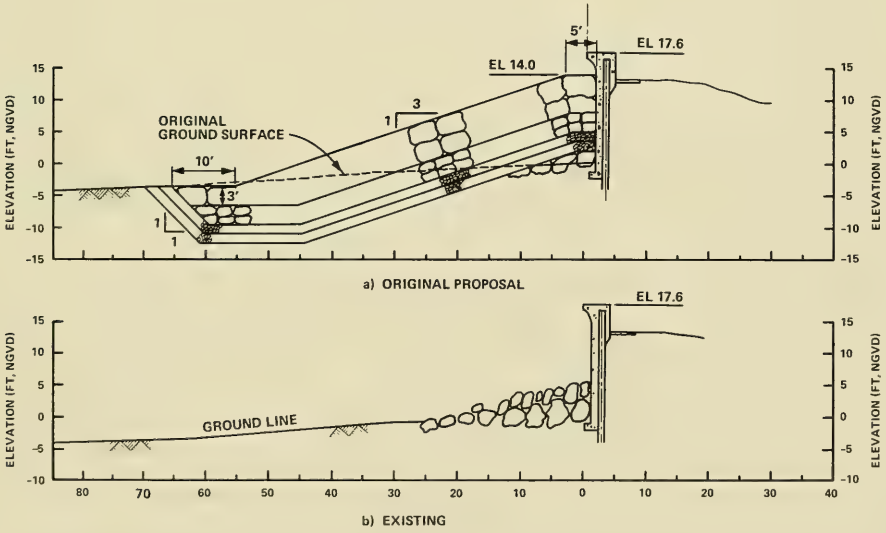

Figure 31. Existing and originally proposed Roughans Point structures for reach E

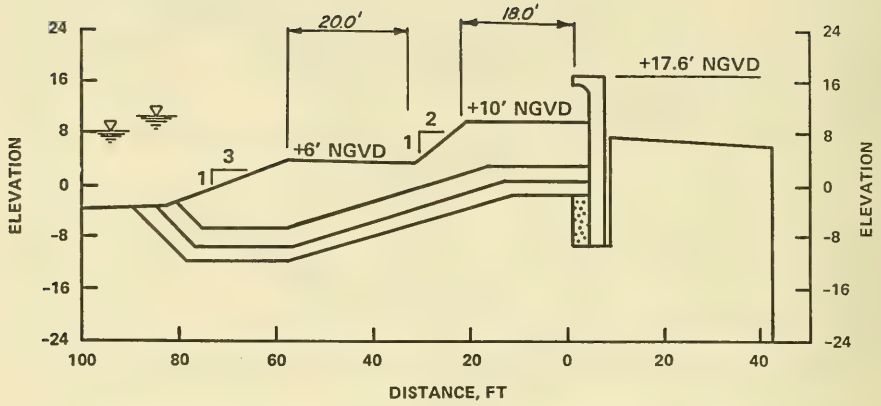

a. Two berms

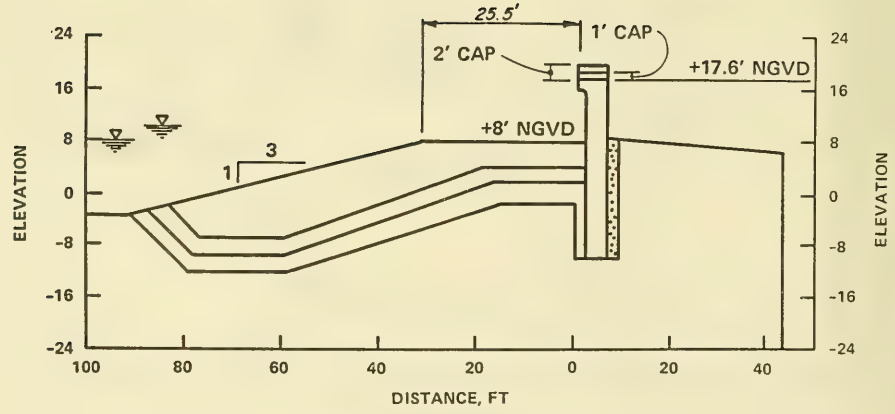

b. Wide berm, wide berm + 1-ft cap, and wide berm + 2-ft cap

Figure 32. Additional reach E structures analyzed

Table 7

Results of Physical Modeling

Test	Wall Height ft, NGVD	Revetment Slope ft/ft	Revetment Height ft, NGVD	Q_0	C_1
North Wall (A,C,D)					
Existing - A	15.3	-	-	3.473	-10.074
- C	13.7	-	-	10.580	-6.776
- D	11.0	1.5	11.0	18.859	-9.762
Original Proposal (A,C,D)	17.0	3.0	17.0	75.189	-17.783
East Wall (E)					
Existing	17.6	-	-	76.554	-14.078
Original Proposal	17.6	3.0	14.0	30.539	-13.431
Two Berms	17.6	3.0*	10.0*	158.240	-25.226
Wide Berm	17.6	3.0	8.0	439.220	-21.621
Wide Berm + 1-ft Cap	18.6	3.0	8.0	305.821	-23.073
Wide Berm + 2-ft Cap	19.6	3.0	8.0	93.037	-22.154

* Two berms (10.0 and 6.0 ft) in this alternative (see Figure 32).

$$Q = Q_0 e^{(C_1 F')}$$

$$F' = \frac{F}{\left(LH_{m_o}^2\right)^{1/3}} \tag{8}$$

where

Q = overtopping rate per foot of structure, cubic feet/sec/ft

Q_0 = coefficient determined from physical modeling, cubic feet/sec/ft

C_1 = coefficient determined from physical modeling

F' = dimensionless freeboard

F = freeboard, difference between still-water level and structure height, ft

L = wave length at structure, ft

Overtopping Rate Calculation

64. A computer code was developed to calculate overtopping rates for both existing and alternative structures for the 150 simulated events. Inputs to this code were time-histories of water level and wave parameters and coefficients from the physical modeling. Output was a time-history (15-min

increments) of overtopping rates at each reach for each event simulated.

65. A check was made to limit the calculated overtopping rates. Assuming that the maximum volume that can overtop a wall (when the freeboard is reduced to zero) is the volume contained between the elevation of the top of the wall and the surface of the wave (Weggel 1976), and assuming linear wave theory with a sinusoidal wave profile, Equation 9 can be derived. The 0.85 factor is included to account for nonlinearity of the real wave form. The condition where Q reached its maximum rate was not common, occurring only at the peak of the most severe events at existing reach D are expressed as

$$Q_{max} = \frac{0.85\ HL}{2\pi T} \tag{9}$$

66. The contribution from wind-aided overtopping was added to the rates calculated from the physical modeling results. This contribution is calculated using Equation 10 (adapted from the SPM (1984, p. 7-44)). Equation 10 is multiplied by 0.30 to account for overprediction.* For wind speeds of 60 mph or greater, $W = 2.0$; for wind speeds equal to 30 mph, $W = 0.5$. When the wind speed is zero, $W = 0.0$. For all other wind speeds W is interpolated from these values. Since wave runup data were not available from the physical modeling, Equation 11 (Ahrens and McCartney 1975) was used to estimate R in Equation 10. Equation 12 shows how the correction for wind aided overtopping is combined with the physical modeling results to produce total overtopping Q_t . Wind aided overtopping was usually less than 10 percent of total overtopping. These equations are written as follows:

$$C_W = 0.3W\left(\frac{F}{R} + 0.1\right)\cos\alpha\cos\beta \tag{10}$$

where

C_W = fraction of overtopping which is wind aided

W = coefficient based upon wind speed

R = wave runup, ft

α = wind angle relative to line normal to structure, degrees

β = structure slope, degrees

---

* Personal communication with John Ahrens, 1985, Wave Research Branch, Wave Dynamics Division, CERC.

$$R = \frac{Ha\chi}{1 + b\chi} \tag{11}$$

where

$a = 0.956$, regression coefficient

$b = 0.398$, regression coefficient

$$\chi = \frac{\tan \beta}{\sqrt{\frac{d}{L_0}}}$$

d = water depth at structure, d

and

$$Q_t = Q\ (1 + C_w) \tag{12}$$

where Q_t is the total overtopping rate per foot of structure in cubic feet per second per foot.

Flood Routing

67. Since the final desired result at Roughans Point is the frequency of the interior water levels, another computer code was developed to route overtopping volumes through the Roughans Point interior. This flood routing code used output from the water level modeling and overtopping rate calculations. Output from the flood routing consisted of the maximum stage calculated for each event. These maximum levels were used for input to generate the stage-frequency curve, for the interior of Roughans Point.

68. For this report the only source of flooding considered was from wave overtopping. Runoff from rainfall was not considered. This will have an effect on the resulting stage-frequency curve, especially at the lower return periods. This contribution will be determined by NED.

69. Outflows from the interior of Roughans Point result from several sources: storm drainage, seepage, pumping, and overflow both into the ocean over low wall sections and into other drainage areas over elevated roadways. Proposed improvements, in addition to providing for reduced rates of overtopping, also include increased storm drainage and pumping. Figure 33 contains a

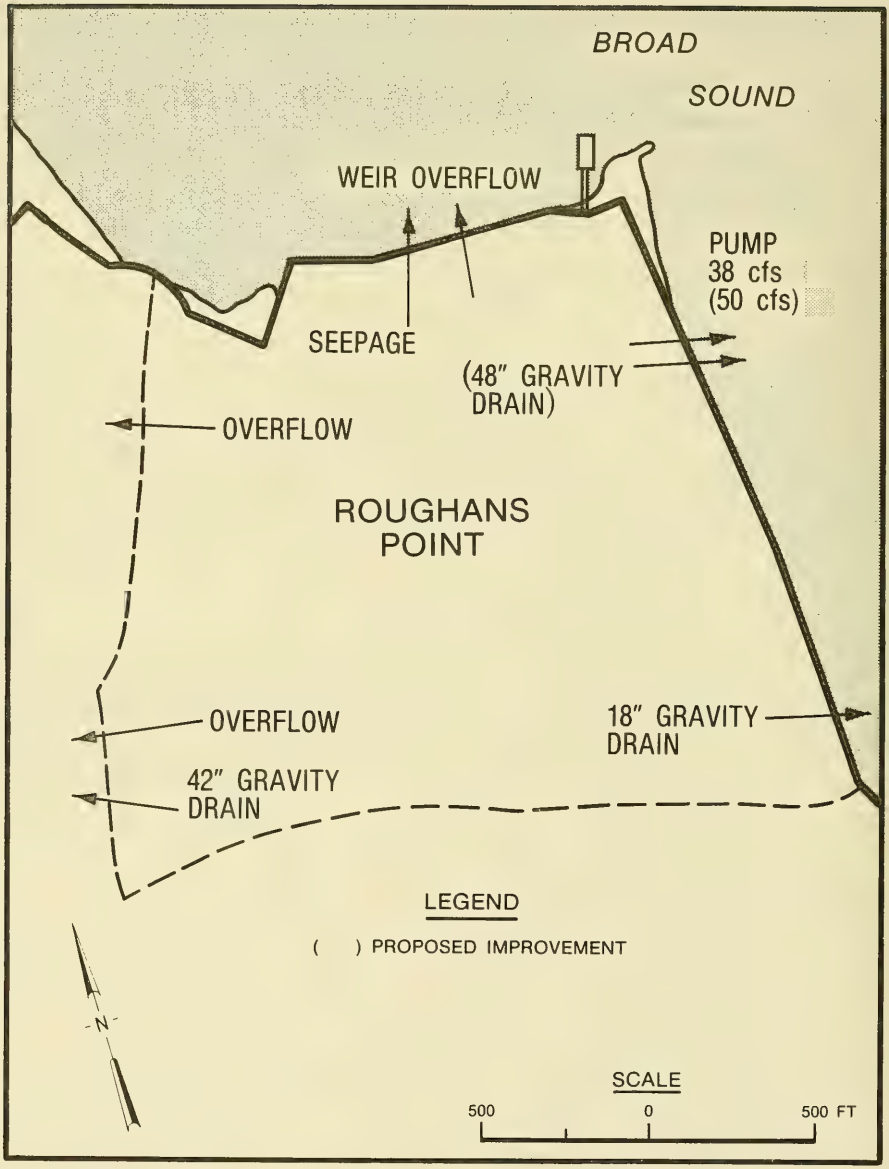

Figure 33. Sources of outflow from the Roughans Point interior

map of the Roughans Point area showing locations of both existing and proposed sources of outflow from the area.

70. There are two existing storm drainage outlets. The largest drain, a 42-in. diam pipe, runs to the west under Revere Beach Parkway at the southwest corner of Roughans Point. The other outlet is an 18-in. diam flat-gated drain which discharges into the ocean at the south end of Broad Sound Avenue. Two proposed improvements, both located at the existing pumping station, are an improved pump intake and a new gravity drain (42 in. diam) into the ocean through reach E.

71. Especially for existing conditions, the water levels inside Roughans Point can reach elevations which are higher than the existing wall at reach D (10.5 ft NGVD). Since the inside water level at these times would be higher than the ocean level, water would flow out over this wall section during peak flooding. This occurs with maximum interior water levels greater than approximately a 40-year return period. Also, at the western edge of the Roughans Point area, there are at least two locations where, at high water levels, water would flow over and under Revere Beach Parkway and into an adjacent drainage area. This outflow was modeled using weir equations.

72. The existing pumping station was built in 1975. The station has three pumps with a combined capacity of 48 cfs. However, with the existing intakes, the capacity is reduced to approximately 38 cfs. As was stated above, proposed improvements to the intakes for the pumping station are planned. The pumping station was inoperative during most of the February 1978 storm because of electric power failure. Also, if a severe storm is forecast the pumping station might not be operational after the evacuation of the area.

73. Loss of water from the interior of Roughans Point will also occur because of infiltration into the ground and seepage through the walls back out into the ocean. The seepage rate should be highest at low tide and when the interior levels are near the top of wall at reach D, where the ground appears especially porous.

74. Four basic equations (13-16) were used in the flood routing calculations. Equations 13-16 and the accompanying coefficients used to calculate the outflows from the interior of Roughans Point during times of overtopping were supplied by NED and were based upon their knowledge of drainage and hydrologic characteristics of the interior of Roughans Point. Drainage and seepage were calculated by Equation 13. Weir outflow was calculated when the

interior water level was higher than a boundary of the Roughans Point area. The weir outflow calculations were accomplished with two separate equations. When the ocean water level is below the height of a boundary, Equation 14 is used. When the ocean level is above the boundary, Equation 15 is used. Equation 16 was used for calculating the outflow due to pumping. Equations 13-16 are expressed as

$$Q_{out} = C_3(S_i - S_b)^{0.5} \tag{13}$$

where

Q_{out} = flow rate in cubic feet per second
C_n = coefficients (3-6)
S_i = interior water level
S_b = the larger of either 4.0 ft NGVD or ocean water level

$$Q_{out} = C_4\,(2.7)(S_i - S_w)^{1.5} \qquad \text{if } S_i > S_w \text{ and } S_o < S_w \tag{14}$$

where

S_w = height of wall section
S_o = ocean water level

$$Q_{out} = C_5(2.7)(S_i - S_w)^{1.5}\left[1 - \left(\frac{S_o - S_w}{S_i - S_w}\right)^{1.5}\right]^{0.385} \qquad \text{if } S_i > S_w \text{ and } S_o > S_w \tag{15}$$

$$Q_{out} = C_6 \tag{16}$$

75. The coefficients which were used in the above equations are shown in Table 8. Coefficients C_4 and C_5 are the length of weir section. Coefficient C_6 is the pumping rate in cubic feet per second. The increase in C_6 for the proposed condition is due to improved inlet design. Coefficient C_3 (see page and drainage) increases for the proposed condition because of the addition of a gravity drain (see Figure 33). Note that two values are listed for coefficients C4 and C5 . For existing conditions, reach D was divided into two sections for this analysis, one section at a height of

Table 8

Coefficients Used in Outflow Equations 13-16

Coefficient	Existing	Proposed
C_3	44	94
C_4	250	--
	575	--
C_5	250	--
	575	--
C_6	38	50

10.5 ft NGVD and the other section at a height of 11.5 ft NGVD (the first and second numbers, respectively). The overflows at the west end of the Roughans Point area are included only in the 11.5-ft coefficient.

76. In the flood routing calculations, the path and time of travel of the water from the time it overtopped the walls until it reached drainage points were not considered. Therefore, all water entering Roughans Point was assumed to be immediately available for drainage. The characteristics of inlets and the capacity of the system were taken into account in the coefficients of Equations 13-16. The flood routing calculations can be summarized as follows. A 1-minute time-step was used. Inflow volumes from wave overtopping from all reaches were combined and then added to the volume remaining from the previous time-step. Outflows were subtracted using the methods outlined in the previous paragraphs. For each time-step the resulting stage was determined from a stage-volume relationship supplied by NED (Figure 34). Finally, the maximum stage during each event was determined for use in stage-frequency generation.

77. Sufficient data were available during two historical events, February 1972 and February 1978, for a rough calibration and verification of the combined overtopping and flood routing process. The maximum interior flood level which occurred during these two events was estimated from water marks and eyewitness accounts. For calibration of the Roughans Point interior calculations, the 1978 event was simulated by the storm surge and wave models. Then the overtopping rates and maximum stage were calculated by the computer codes described above. The first attempt predicted interior stages which were in excess of those observed; therefore, refinements and adjustments, discussed

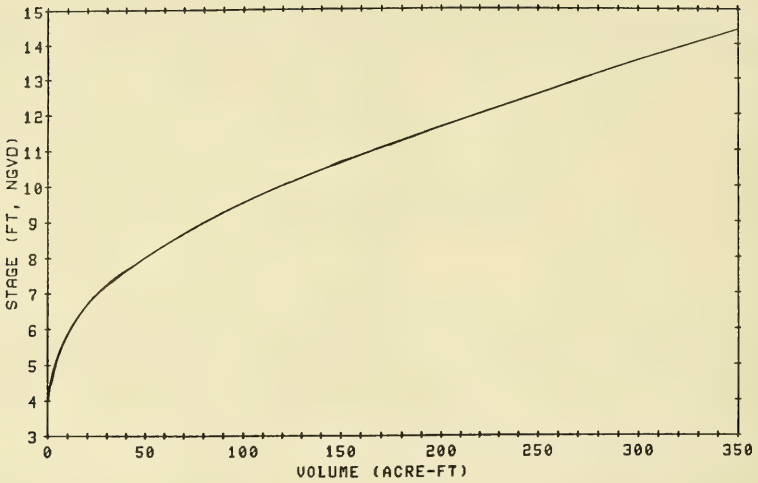

Figure 34. Stage volume versus volume relationship for Roughans Point interior

in the following paragraphs, were made to match the estimated stages.

78. For existing conditions, overtopping at reach D was not allowed during periods of weir outflow at that wall. Since there would be a continuous current flowing outward in this situation, it was reasoned that any overtopping would almost immediately be conveyed back into the ocean. Without this reasoning, reach D would contribute enormous quantities of overtopping at those times when Roughans Point was full to overflowing. This assumption is consistent with the limited information available from the only historic event, in February 1978, during which the water level inside Roughans Point was higher than the elevation of reach D.

79. Wave heights attacking reach E were reduced by 15 percent. There were several possible adjustments which could have been made to eliminate overprediction of overtopping rates. Among these are (a) reducing the calculated overtopping rate, (b) lowering the still-water level, and (c) reducing the wave heights. The wave heights were selected for reduction because they are the least certain of these possibilities (see "Estimating Error in Stage-Frequency Curves" in Part VI).

80. Wave heights were also lowered for the three northern reaches. At

reach D , the height of waves which propagate from the open ocean was set to zero. There were two justifications for this adjustment. First, due to the orientation of the wall, there is no opportunity for these waves to attack the wall from any but very oblique angles. Second, reach D would be partially sheltered from waves from these oblique angles by the tip of Roughans Point and by Simpson's Pier. At reaches A and C, waves from the open ocean were reuced by 50 percent. As at reach D, these waves would approach from an oblique angle; however, refraction would turn these waves more normal to reaches A and C than at reach D. Since the physical modeling assumed a wave direction normal to the structure, using the full wave height for these waves would result in the overprediction of overtopping rates. The locally generated waves were reduced by 15 percent for all three north wall sections. This can also be justified by the fact that these waves do not always approach normal to the wall sections.

81. The above adjustments were made to the overtopping calculation and flood routing computer codes to match calculated values of interior stage to those observed during the February 1978 storm. The February 1972 storm was then simulated to verify the revised procedure. The results of these two simulations are compared to estimates of actual flooding in Table 9.

Table 9

Comparison of Calculated to Observed Flood Stage

Storm	Calculated ft, NGVD	Observed ft, NGVD
1978	11.9	11.8-12.0
1972	9.6	8.8-9.0

82. The results of this calibration and verification were judged to be acceptable. The 0.6-ft difference between observed and calculated water levels for the 1972 storm seems reasonable when considering that the calculations were based upon a stage-volume relationship determined from 2-ft contour intervals.

Simulation of the Event Ensemble by the Flood Routing Model

83. Following calibration and verification of the flood routing model,

events were simulated for the existing one and five alternative structure combinations. Inputs to the model were the time-histories of overtopping rates for each of four Roughans Point reaches (A, C, D, and E). Six different combinations of the northern and eastern reach structures were modeled. Since the north wall has only two structure classes, "Existing" and "Original Proposal," a combination of northern and eastern structures was given the name of the eastern structure. The "Existing" combination is self-explanatory. The "Original Proposal" combination is made up of the northern and eastern structures proposed before the beginning of modeling (see Figures 28-31 and NED 1983). The other four alternatives, "Wide Berm," "Two Berms," "Wide Berm + 1-ft Cap," and "Wide Berm + 2-ft Cap," combined the eastern structure of the same name (see Figure 32) with the northern "Original Proposal" structure. There were two output files. One file was a time-history of flood stages for each event and structure simulated. The second file contained the maximum stage during each event for each combination of structures simulated. This second file was used to compute the stage-frequency curves.

North Wall Tests

84. During the course of simulating overtopping and flood routing, there was no contribution to overtopping volumes from the "Original Proposal" northern structure. Tests were conducted to determine the effect of lowering the height of the protection along the whole north side of Roughans Point. Since no additional physical model tests were to be run, a method had to be devised to use physical model data from the proposed northern structure (17 ft). Reconsideration of the overtopping rate equation (Equation 8), reveals that changing the height of the northern structure would only change one term in that equation, namely F_c, the freeboard. Since the water level would not be changed, the characteristics of the waves attacking the structure would not be changed. Therefore, even though lower heights were not tested, estimates of the overtopping for lowered structure heights could be made by reducing the freeboard in Equation 8. Using the February 1978 historic event for the initial tests, the northern structure was lowered in 1-ft increments. For this event, overtopping did not start until the structure was lowered to 14 ft NGVD, and large volumes of overtopping did not commence until a structure height of 12 ft NGVD was tested. Using these results, the full ensemble

of 150 events was simulated for northern structure heights of 14, 13, and 12 ft. The results of these tests are presented in Part VII.

PART VI: STAGE-FREQUENCY CURVES

85. In this section, the method for establishing stage-frequency curves will be described for both the still-water locations and for the interior of Roughans Point.

86. The goal of this project was to produce stage-frequency curves for two distinct processes. The first process involved the interaction of storm surge and tide to produce still-water levels at coastal (and river) locations, and the second process combined waves with the surge and tide to produce flood levels behind seawalls due to wave overtopping. Although the simulation of these two processes involved some different steps, development of frequency curves for the two processes once the water levels are determined is essentially the same.

87. Probability was assigned to each of the events selected for simulation, as described in Part II. By assigning the probability to the maximum still-water level caused by the event at each numerical gage location, stage-frequency curves can be constructed by the following method. First, an array of possible stages at each gage location is established with a discretization interval (0.1 ft for this project). Next, for all 150 events, the probability masses assigned to each event are accumulated in the stage interval which brackets the maximum water level that occurred for that event. Exceedances can be determined for any interval by adding the probability of that interval to the sum of the probabilities of the intervals above it. After this was accomplished for the total set of 150 events, the process was repeated for each of the three sets of 50 events. This produced three additional sets of stage versus exceedance relationships which were used for confidence calculations.

88. The range of stages modeled in the still-water level portion of this study was just over 3 ft (from 7.9 to 11.2 ft NGVD). All of the resulting 33 discretization intervals did not receive probability. Some intervals received probabilities from several events causing in places (in the array of stages) a series of heights where no event deposited its probability. This occurrence results in a jagged line when the stage-frequency is plotted.

89. There is no physical reason why adjacent height intervals should have greatly different probabilities. The jagged nature of the raw curves is caused by trying to represent a continuous process (all possible storm events)

with a discrete process (50 storm events). Modeling more events would result not only in a smoother curve but also in greater expense. For example, had 500 events been modeled, it would be highly unlikely that one height interval would receive the probabilities of several events while the three intervals below received none. Therefore, if an economically feasible number of events were to be modeled, the raw output of the stage-frequency generation would require smoothing to adequately represent a continuous curve.

90. Smoothing was accomplished using linear regression of the stage-frequency data when plotted on an appropriate probability paper. Equation 17 is a formula for the construction of Weibull probability paper. Where

$$x_{new} = \left[-\ln\ (x_{old})\right]^{c} \qquad (17)$$

the variable x_{old} is the inverse return period, x_{new} is the transformed abscissa value, and c is the variable to be adjusted to best represent the data with a straight line. After numerous trials a c value of 0.80 was chosen. Figure 35 contains a plot of both the raw and regressed stage-frequency curves for the Fox Hill Drawbridge still-water location.

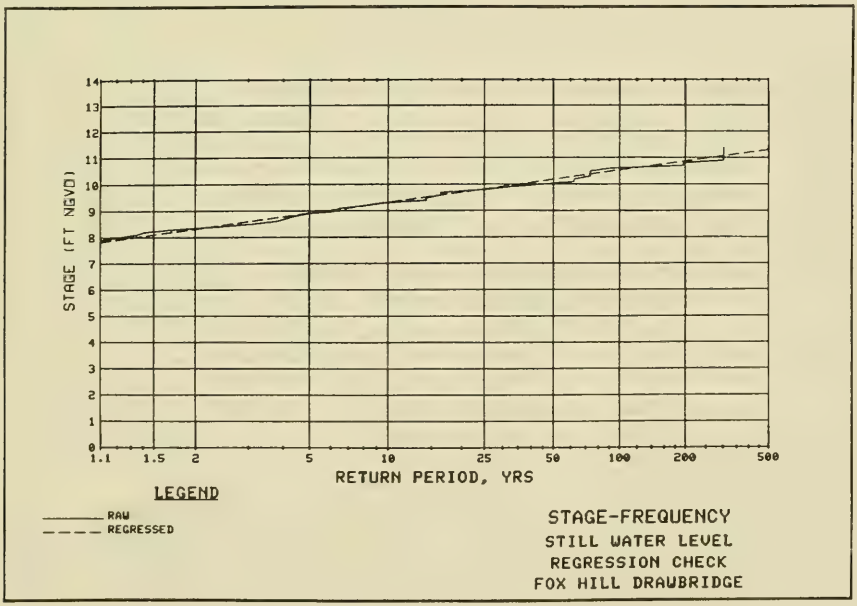

Figure 35. Example of raw and regressed stage-frequency curve

Roughans Point

91. The stage-frequency curves for the interior flood levels in Roughans Point are presented in Figures 36-40. For these curves it was not possible to regress the total curve as was explained in Part VI. The physics of the problem undergoes a sudden change at higher levels where the effect of weir outflow limits the capacity of the interior of Roughans Point. Also the extreme lower portion of the curves does not conform to the straight line tendency of the middle portion. The lowest possible stage is 3.6 ft NGVD corresponding to the lowest point inside Roughans Point. Consequently, the stage-frequency curves remain at 3.6 ft until the onset of overtopping. Therefore, the linear regression was limited to the middle segment of each curve for the Roughans Point stage-frequency curves. Smoothing for both the lower and higher segments of the curves was done by eye.

92. As explained in paragraph 83, flood levels were calculated for six different combinations of northern and eastern structures. The names of the structure combinations plotted in Figures 36-40 refer to the names of the eastern component. (For the "Existing" and "Original Proposal" structures (NED 1983) refer to Figures 28-31, and for the other alternatives refer to Figure 32.) Three tests lowering the height of the proposed north wall structure were conducted. Since it was determined that there was a negligible difference between the curves with the originally proposed north wall height (17 ft NGVD) and the curves from the highest of the three additional tests (14 ft NGVD), curves resulting from the 17-ft height are not presented. Curves for the six structure combinations are shown in Figures 36-38, with the height of the northern structure in the three figures being 14, 13, and 12 ft, respectively. Note that the 14-, 13-, and 12-ft north structure heights refer only to the alternative structure combinations. For the "Existing" curve, shown on these graphs for comparison purposes, the northern structure is set at the existing height for each structure section.

93. Using Figure 36, several features of the stage-frequency curves for the interior flood levels at Roughans Point will be discussed. The greatest differences among the alternatives occur at the lower return periods. Near the 500-year return period all six curves tend to come together. As was

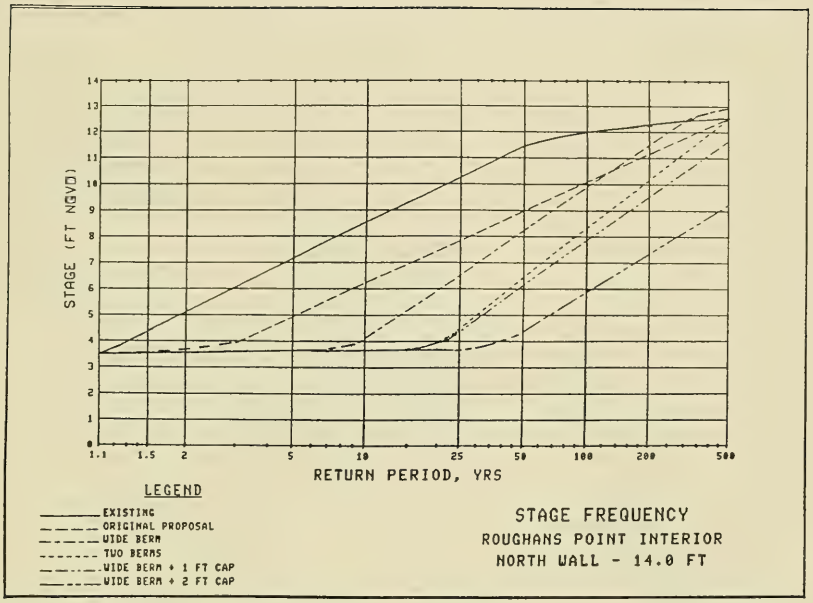

Figure 36. Roughans Point stage frequency, northern structure height = 14 ft

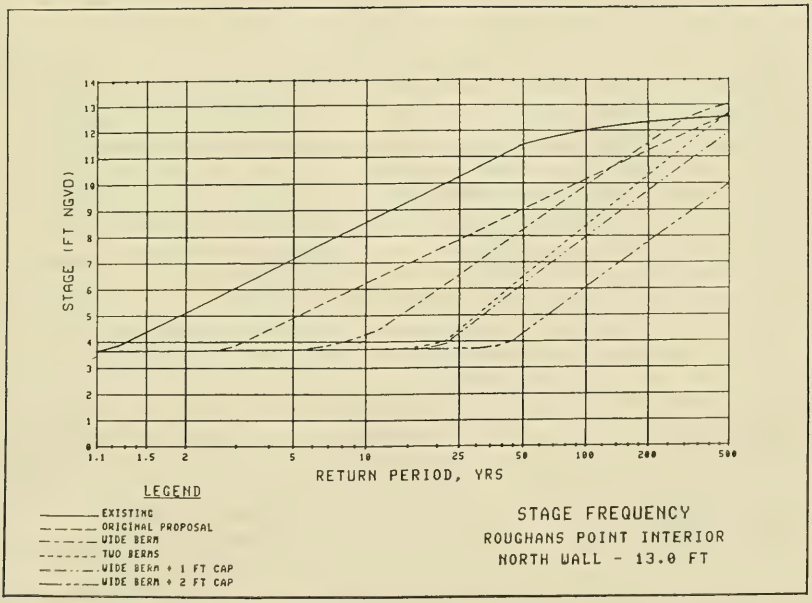

Figure 37. Roughans Point stage frequency, northern structure height = 13 ft

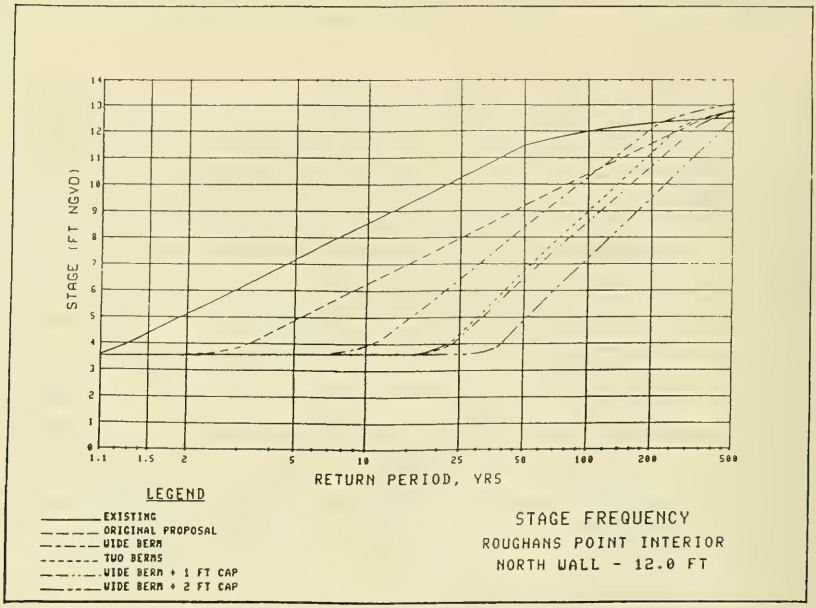

Figure 38. Roughans Point stage frequency, northern structure height = 12 ft

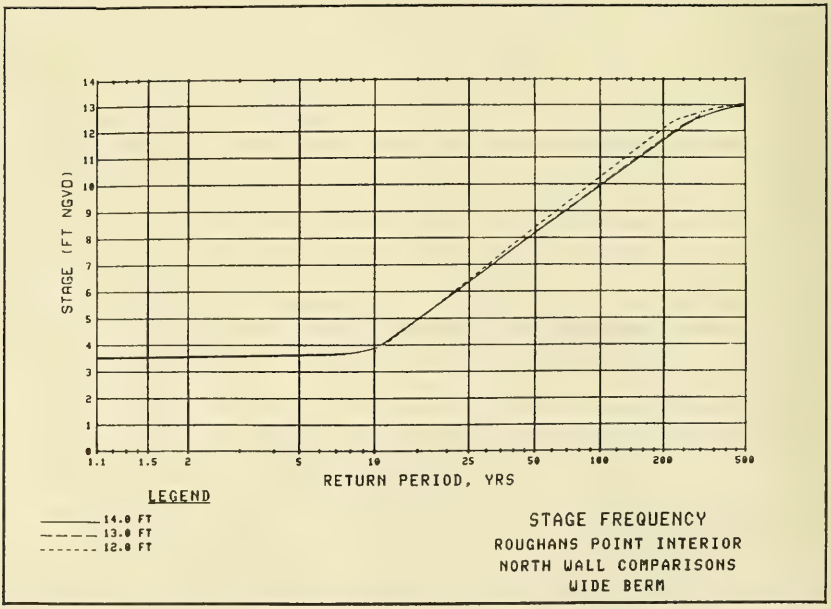

Figure 39. Effect of northern structure height on the "Wide Berm" alternative

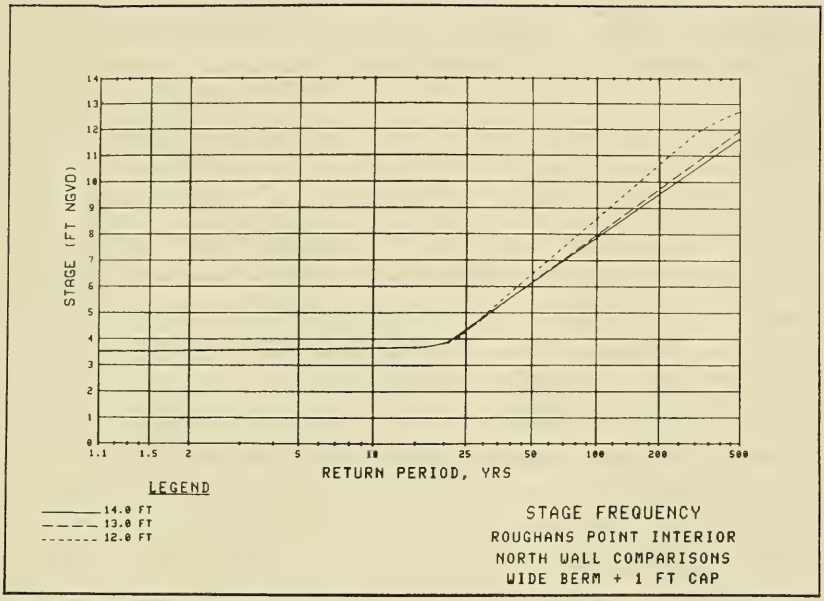

Figure 40. Effect of northern structure height on the "Wide Berm + 1-ft Cap" alternative

discussed in Part V, Roughans Point has a limited volume capacity. When the amount of overtopping surpasses the capacity of the interior, the water pours out over roadways into another drainage area. Therefore, although the various alternatives are still producing very different overtopping rates, the flood levels that result are similar for the highest return periods.

94. Although the "Two Berms" alternative produced results very similar to the "Wide Berm + 1-ft Cap" alternative, the "Two Berms" structure is not a recommended alternative. The physical model tests showed the "Two Berms" structure was not stable. For details see Ahrens and Heimbaugh (in preparation).

95. The wide berm configuration proved to be effective in lowering overtopping at the still-water levels which accompany return periods less than 100 years. Notice, however, that in Figure 36 the "Wide Berm" curve crosses above the "Original Proposal" curve at about 150 years. The berm loses its effectiveness in reducing overtopping as the higher still-water levels submerge it.

96. The effectiveness of the berm is dramatically improved by adding

height to the wall behind it, as is seen in both the "Wide Berm + 1-ft Cap" and the "Wide Berm + 2-ft Cap" alternatives. Studying the overtopping rate equation (Equation 8) shows that the overtopping relationships developed from the physical model are very sensitive to freeboard and, therefore, to structure height.

97. Recommending a height for the north wall is difficult. None of the three heights were actually modeled by the physical model. The final structure selected must, of course, result from a detailed economic analysis. The technique of using the 17-ft north wall physical model results to predict the results for lower revetment heights by lowering freeboard was the best available but must lower confidence in the analysis. The choice seems to be between the 13- and 14-ft heights. The 12-ft height allows significantly greater overtopping to occur. Figures 39 and 40 show the effect of north wall height on the "Wide Berm" and the "Wide Berm + 1-ft Cap", respectively. Since the height of the existing wall sections at A and C (15.3 and 13.7 ft NGVD) is higher than that of the 13-ft trial, the best choice would be a revetment at a 13-ft height with the wall keeping its existing height at A and C, with the height at B being a transition between A and C, and the height at D matching that at C.

Still-Water Locations

98. Stage-frequency curves for 14 locations within the Saugus-Pines River system and the coastal areas bordering Broad Sound are presented in Figures 41-54. Figure 23 shows the location of these 14 numerical gages. Just prior to the completion of the study, additional data were collected by NED during the highest predicted tides of September, October, November, and December 1985 for several locations in the extreme upriver portions of the modeling area (Figure 55). Because of increased interest in flood protection for these areas, it was hoped that the additional data would allow adjustment of the modeling results upstream of where calibration data were previously available. Data were collected also at the Fox Hill Drawbridge calibration gage location, and data for the Boston tide gage were obtained from NOS. These data are summarized in Table 10.

99. Based on the information shown in Table 9, adjustments were made to those numerical gage locations west of the abandoned highway embankment and

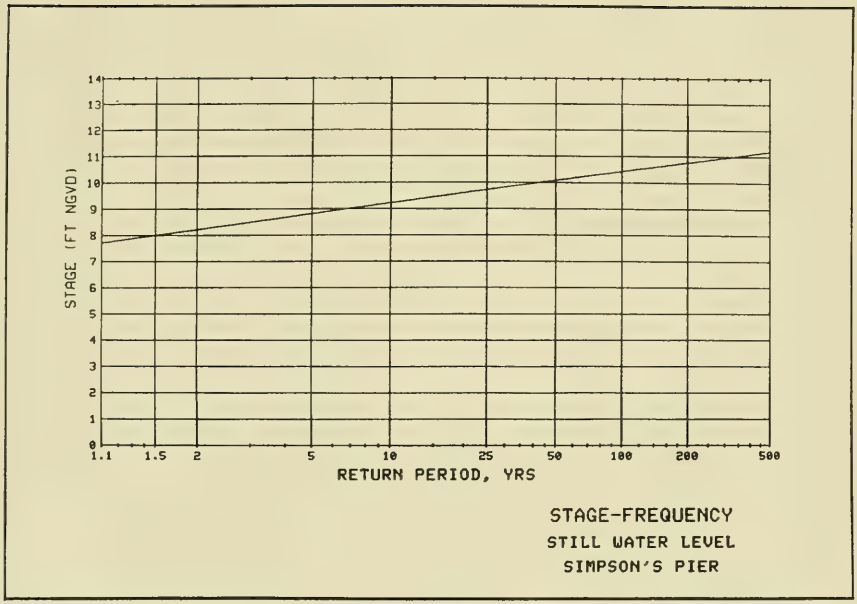

Figure 41. Still-water level stage-frequency curve, Simpson's Pier

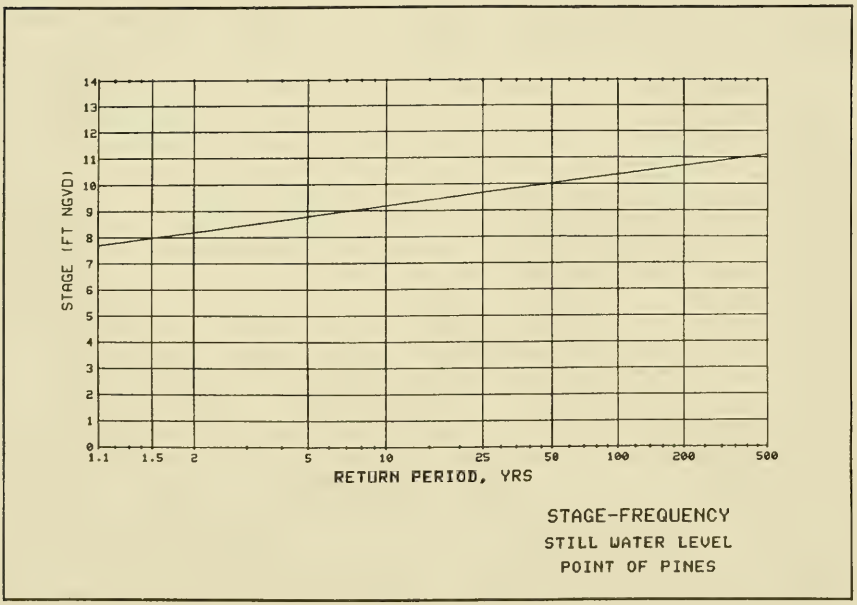

Figure 42. Still-water level stage-frequency curve, Point of Pines

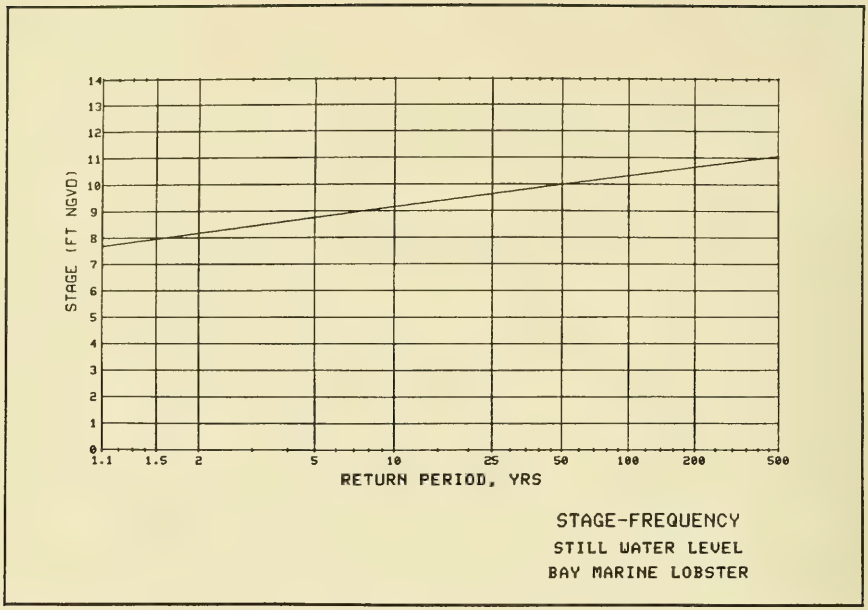

Figure 43. Still-water level stage-frequency curve, Bay Marine Lobster

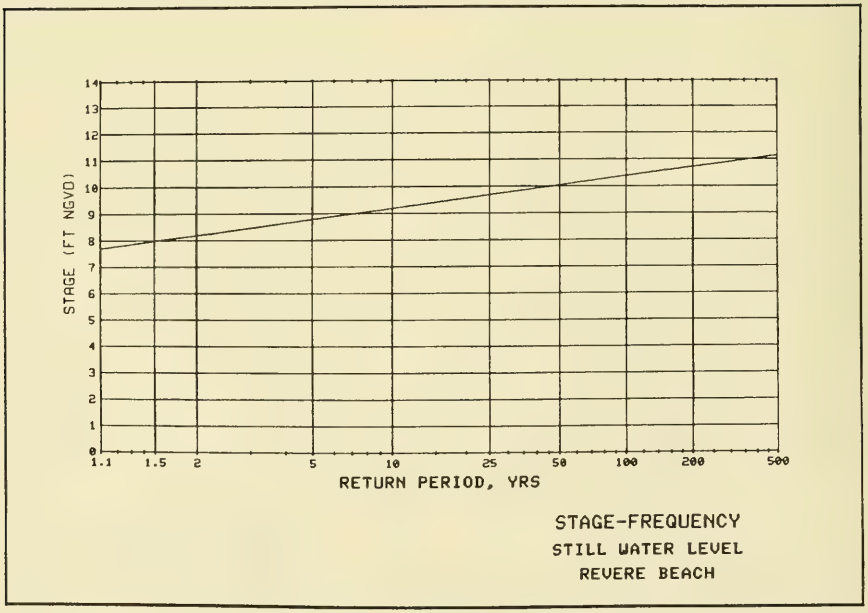

Figure 44. Still-water level stage-frequency curve, Revere Beach

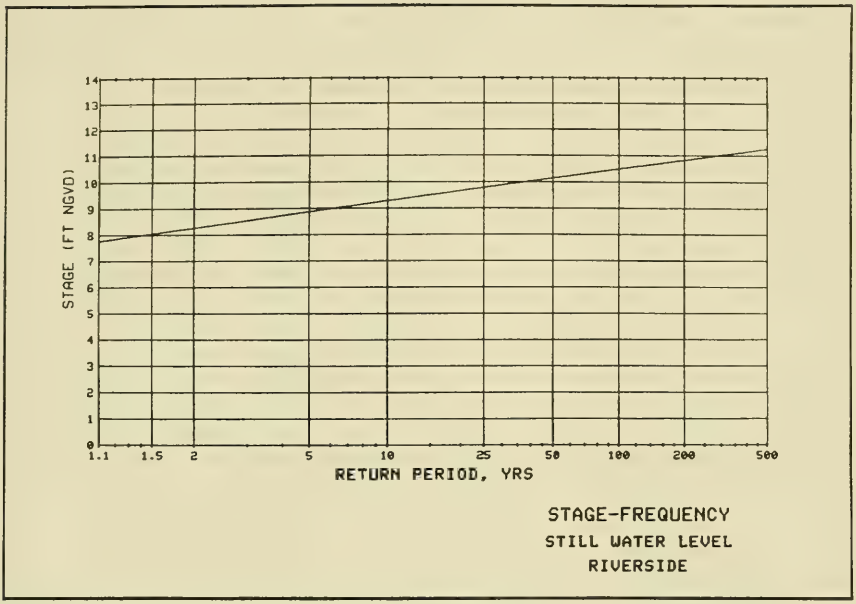

Figure 45. Still-water level stage-frequency curve, Riverside

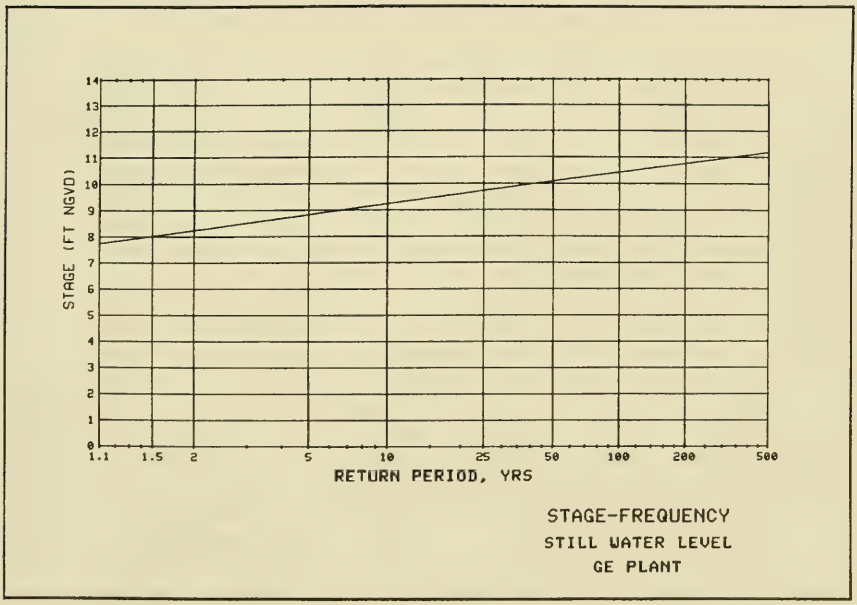

Figure 46. Still-water level stage-frequency curve, GE Plant

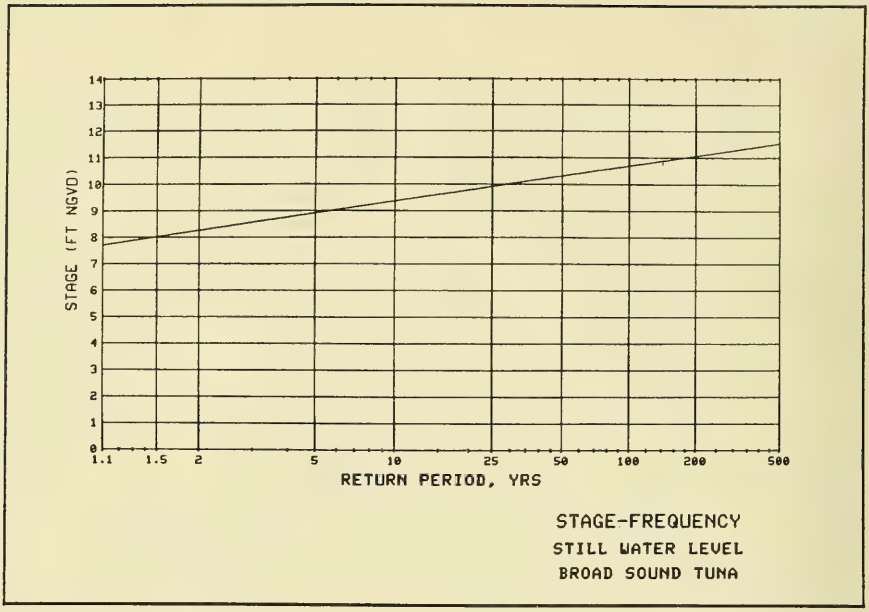

Figure 47. Still-water level stage-frequency curve, Broad Sound Tuna

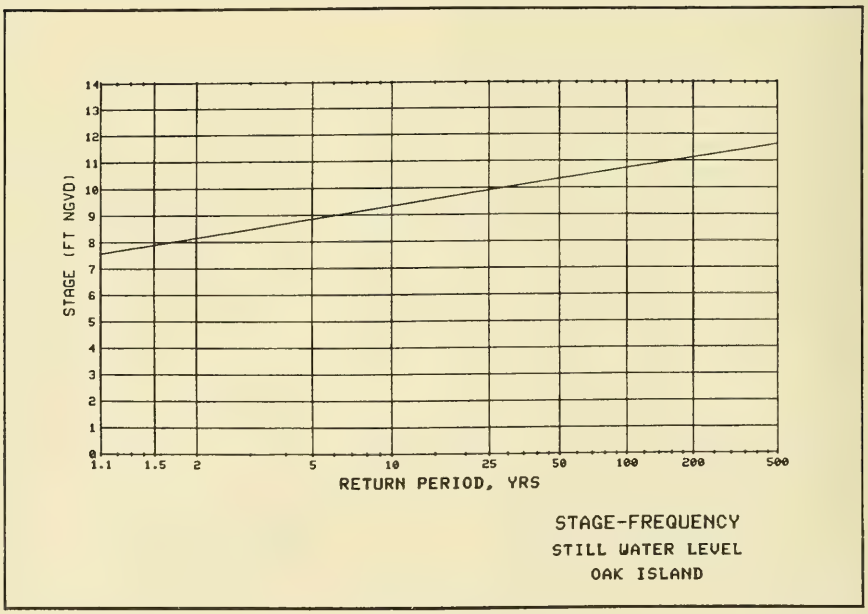

Figure 48. Still-water level stage-frequency curve, Oak Island

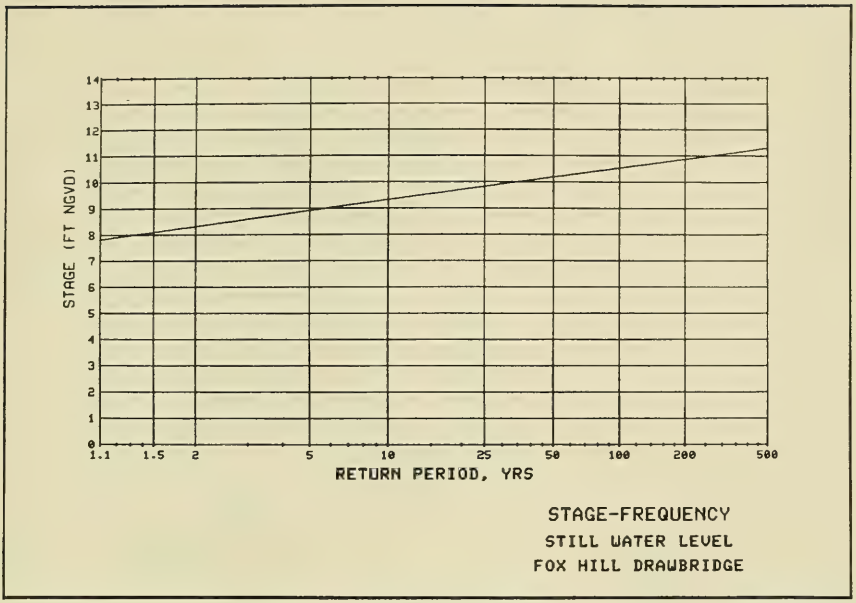

Figure 49. Still-water level stage-frequency curve, Fox Hill Drawbridge

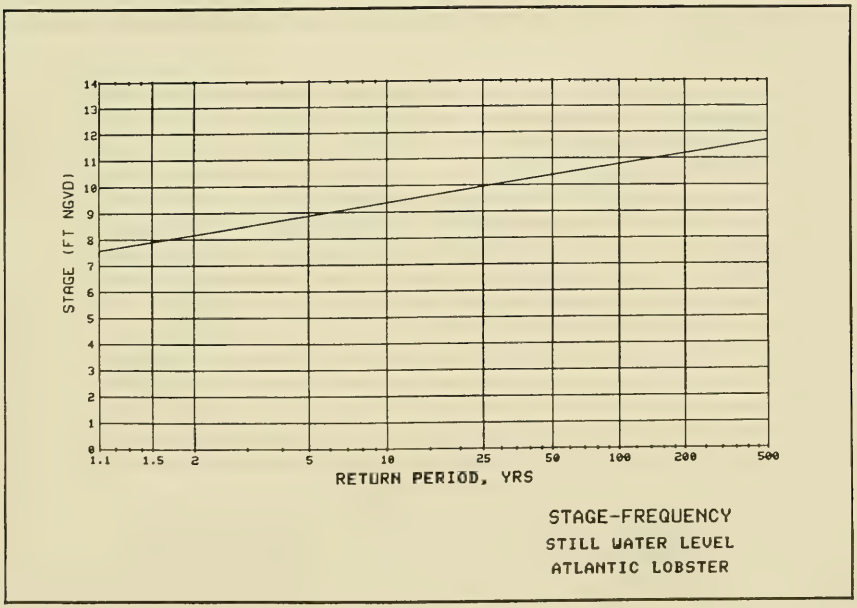

Figure 50. Still-water level stage-frequency curve, Atlantic Lobster

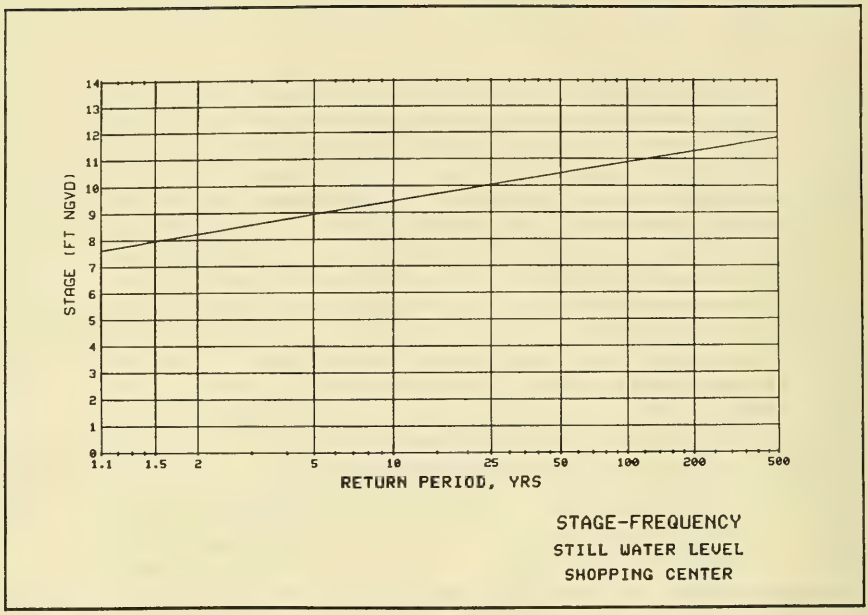

Figure 51. Still-water level stage-frequency curve, Shopping Center

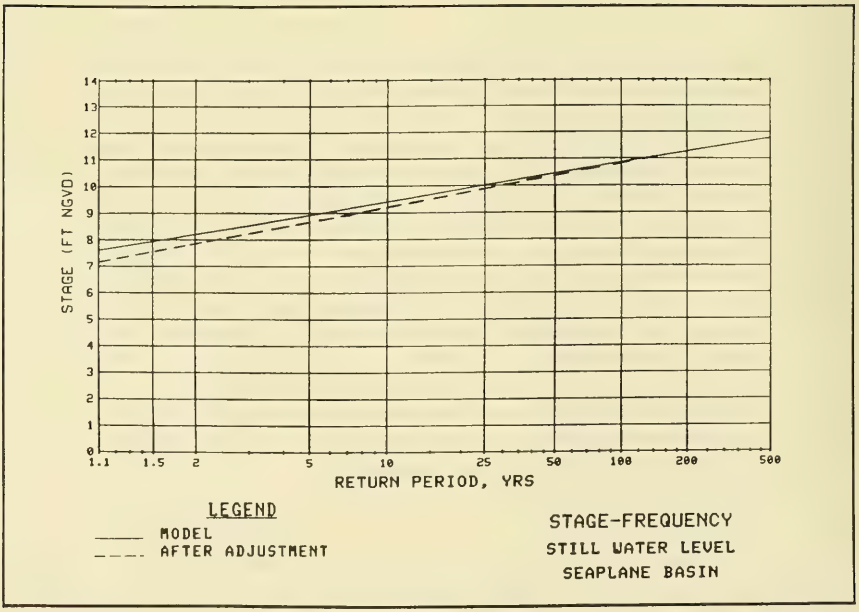

Figure 52. Still-water level stage-frequency curve, Seaplane Basin

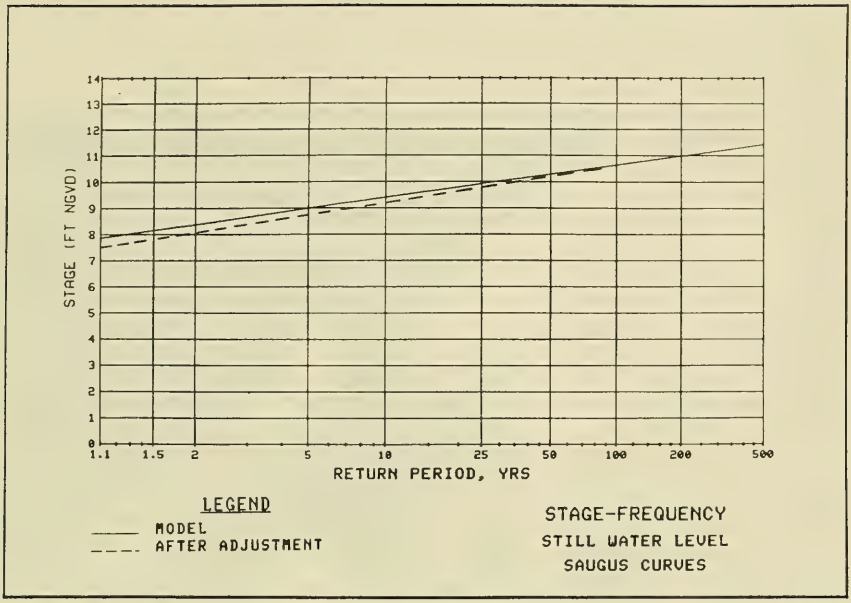

Figure 53. Still-water level stage-frequency curve, Saugus Curves

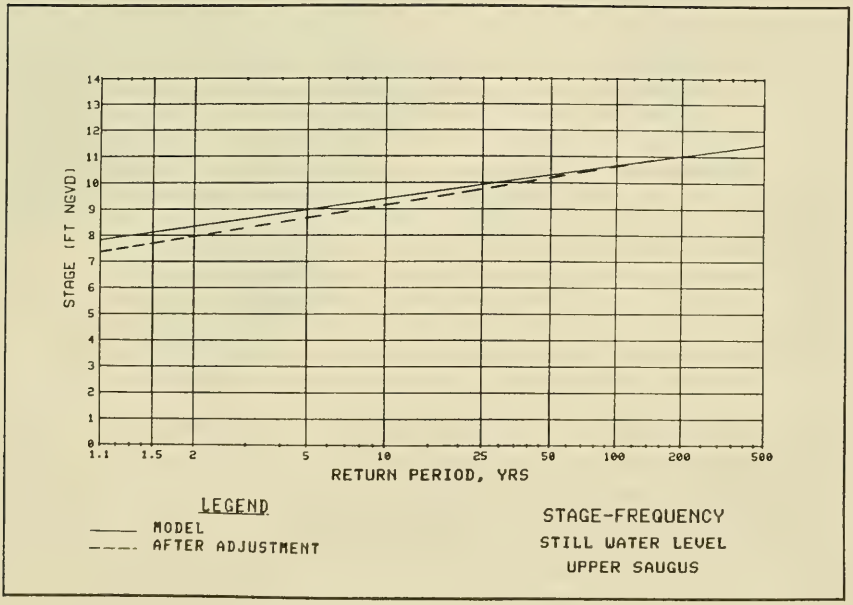

Figure 54. Still-water level stage-frequency curve, Upper Saugus

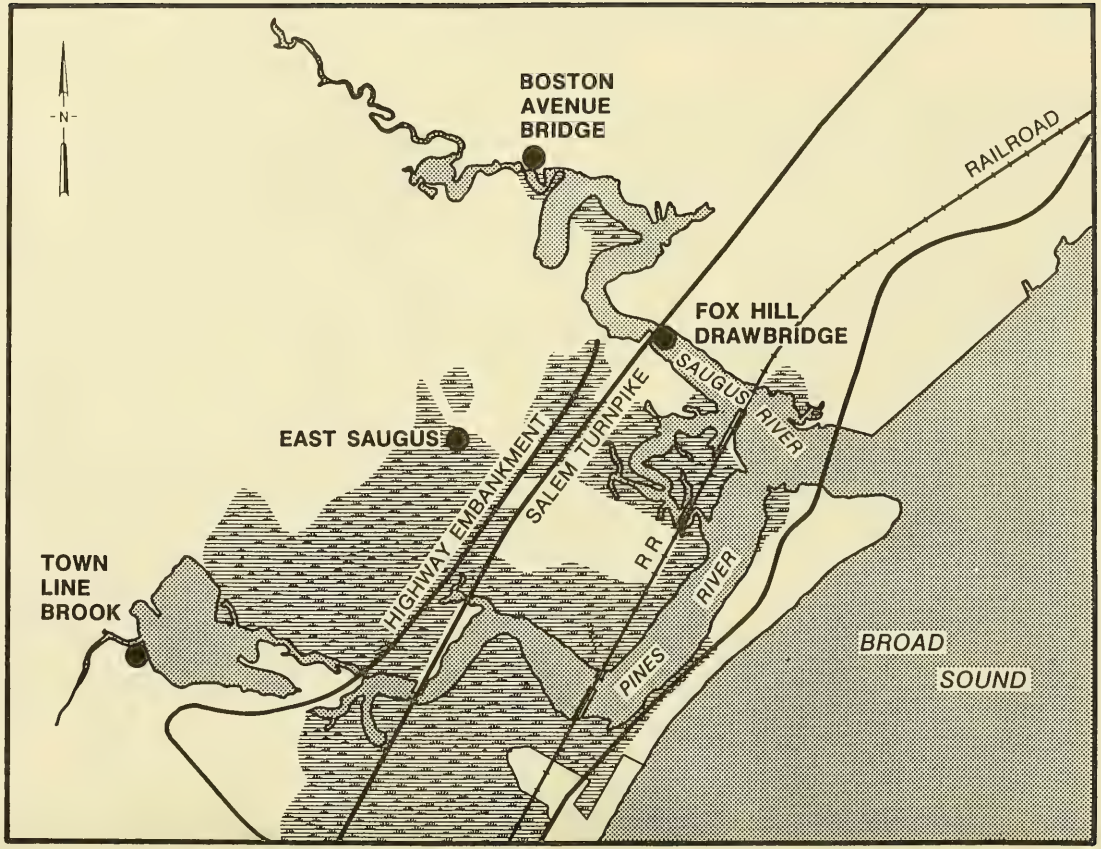

Figure 55. Locations of additional water level data collection

Table 10

Maximum Tide Elevation* Data for Upstream Areas

Location	Date 9-17-85	10-15-85	11-13-85	12-12-85
Boston	6.19	7.44	7.20	8.01
Fox Hill Drawbridge	6.55	7.65	7.15	8.1 (est.)
Boston Ave. Bridge	6.1	7.35	6.95	7.9
Town Line Brook	6.1	7.1	6.65	--
East Saugus	--	--	--	6 (est.)

* All elevations are for the maximum elevation and are in feet referenced to NGVD.

upstream of the Fox Hill Draw Bridge. For areas west of the embankment, the curves were lowered by 0.5 ft at 1.5 years, and a straight line was drawn between this level and the original curve at 200 years. The same adjustment was made for the areas west of the drawbridge, except the reduction at 1.5 years was 0.3 ft. The adjustments were phased out at the higher water levels because, as the water level increases, the access of floodwaters to the back locations in the study area improves. The effect of storm surge is to raise the sea level upon which the tide propagates. Unlike a hurrricane surge time-history, which can be sharply peaked because of rapid changes in both speed and direction of the winds, the time-history of almost all the northeaster surges is very broad with any rapid fluctuations in water level confined to several tenths of a foot. At these higher water levels channel cross sections are increased, the effect of bottom friction is lessened because of greater depths, and new paths of access are created from the overtopping of barriers (roadways). All these factors would tend to negate losses seen in Table 9 for higher water levels. The adjustments to the above mentioned areas are shown as the dotted lines in Figures 52-54.

100. Differences among the curves presented in Figures 41-54 are small. This small difference is not surprising considering the small size of the area being modeled. In general, the curves are slightly higher for locations inside the Saugus-Pines River system as compared to locations in Broad Sound. The predominant wind directions during severe northeasters are from the northeast to north. On the inside of the inlet, these directions would tend to

push water up the Pines River away from the inlet, pumping more water into the river system. Curves for locations upstream on the Pines River would be further increased by the effect of the wind setting up the water over the shallow marsh areas. In general there was a small north to south gradient in flood levels with the more southern areas higher by one-half to three-fourths of a foot during the more severe events. For the Broad Sound locations a smaller variation of a few tenths of a foot with the higher levels at the more southern locations also is explained by the direction of the winds.

101. Stage-frequency curves are not presented for the marsh areas west of the highway embankment. Modeling the routing of the floodwaters in these areas is beyond the scope of this study. For lower return periods observations indicate there is a head loss as the waters go north from the Pines River channel across the Saugus Marsh. In these areas, at lower return periods, flow is contained in drainage ditches which are too small to model with the present grid resolution. Also, other subgrid effects such as localized areas of high ground which could thwart the movement of floodwaters are important but were not considered.

102. It is important to emphasize that the effects of ice and snow were not taken into account by the storm surge modeling. It is possible and perhaps even likely that severe northeasters would be accompanied by heavy accumulations of snow and ice formation in the river systems. Snow banks formed from the clearing of roadways could act to divert floodwaters and provide some measure of protection to some areas. Ice could restrict bridge and channel openings and, therefore, reduce the amount of water entering back areas. Ice cover of open water would likely reduce the wind setup of the marsh areas. Although the above mentioned effects indicated the effect of ice and snow would be to reduce flood levels, scenarios are possible where the opposite would be true. For example, ice could divert the flood into areas which would not have been affected without the diversion.

Estimating Error in the Frequency Curves

103. The final products of this study are curves which depict stage versus return period for flood levels at many locations throughout the study area. At any one return period, say 100 years, the curve is merely an estimate of the true flood level. Moreover, this estimate is only a point

estimate which represents a random variable which has a probability distribution. If this probability distribution can be determined, confidence intervals could be calculated by specifying the probability that the true flood level lies between a range of heights about the estimated value. Confidence intervals are relatively easy to determine when dealing with a single data set, for example, confidence intervals about the mean value of a set of data. However, the calculation of stage-frequency curves as done in this study involves multiple data sets and multiple modeling systems. Even if it were possible to determine confidence intervals about each of the processes separately, there would still be the problem of combining separate intervals into one interval for the final stage-frequency curve. The total 90 percent confidence interval would not be the sum of the 90 percent confidence intervals of all the processes. For example, the storm surge model may overpredict, the wave model underpredict, and the probability model assign too low a probability. Consequently, no attempt will be made to place error bounds on the final curves. Instead, a verbal description of the types and, where possible, the magnitudes of the various sources for error will be given. A method has been developed to show curves for the error associated with the process of selecting a limited number of events to be modeled from the infinite number of possible events. Since the physical modeling was not a part of this report, no attempt will be made to determine the potential for error from the physical modeling. The reader will have to analyze the following paragraphs and determine how the possible error will influence any engineering decisions.

104. The modeling of still-water level involved three main parts: data collection and analysis, numerical model calibration, and simulation. The tide gage data used in the project were carefully screened to remove spurious data points; therefore, this information was probably corrected to about 0.1 ft. Calculating accurate tide time-histories was difficult. Five sets of tidal constituents, each based on an analysis done for a different time period, were tested. Due to the large tidal range at Boston, slight errors in the phase of the predicted tide can cause significant errors when calculating the storm surge time-histories. The storm surge time-histories used for combination with tide were edited by eye to remove any errors caused by poor tide prediction. The numerical grid, as shown by the calibration results, had sufficient resolution to accurately model tide in the areas where calibration data were available. WIFM has performed well in numerous studies, and the

calibration and verification in this study produced excellent results. The one-grid system used in this project should prove to be much more accurate than a two-grid system because of the lack of wind data needed to force an outer grid. The major source of potential error in the water level modeling is the lack of storm data for calibration of the model. Implicit in calibrating the model to tide alone is the assumption that the magnitude of the storm surge at the Boston tide gage is very close to the magnitude of the storm surge in the study area for any storm event. Because the two locations are so close to one another in comparison to the size of either the continental shelf or the size of a typical northeaster, this assumption is probably more accurate than the alternative of using a two-grid system. Taking all these factors into account, it is estimated that the accuracy of any one simulation of the storm surge model would be within a few tenths of a foot in areas close to the tide gages and within about one-half foot in those areas west of the highway embankment.

105. The wave modeling portion of the project was less accurate than the water level modeling for four main reasons. First, the state of the art in wave modeling, particularly in shallow water, is not as advanced as in surge modeling. Second, the numerical wave model used is more recent than WIFM and, therefore, less well tested. Third, there were no wave data available for either calibration or verification of the model. And, fourth, the boundary conditions for the wave modeling (the WIS hindcasts which are the best available) were not as accurate as the gage data used for the water level modeling. These four factors are somewhat offset by the fact, that, for all the more severe wave conditions and for many of the times when overtopping occurred at Roughans Point, the waves approaching the wall were depth limited.

106. The flood routing model contained a series of assumptions for calculating outflow from the interior of Roughans Point. For the flood levels bracketed by the 1972 and 1978 floods, the flood routing model should produce good results. However, for extreme floods, the interior water level is heavily dependent upon the volume of water leaving the interior by flowing over roadways and, for existing conditions, over reach D. Therefore, flood levels higher than those produced by the 1978 event are more uncertain than are lower flood levels.

107. The probability model contained several processes which could potentially introduce error into the final curves. These included assigning

probability from the NED Boston stage-frequency curve, selecting events to model, and fitting a curve to the raw modeling results.

108. It is beyond the scope of this report to assign error bounds to the NED stage-frequency curve. However, a simple investigation of the possible error in the curve would be as follows. The curve was based upon 131 years of record, 57 of which were from a continuous record at the NOS tide gage. Because of the relatively long record, the bottom portion of the curve (i.e. return periods of less than 15 years) should be very accurate. The middle portion of the curve (i.e. return periods between 15 and 100 years) is within the length of record and should be accurate to within a few tenths of a foot. The portion of the curve above the 100-year return period would be more uncertain with, of course, the uncertainty increasing with return period. However, because of the extremely flat nature of the curve (there is only a 1-1/4 ft difference between the 50- and 500-year levels), it seems safe to predict that the curve should be accurate to within a half foot even at the 500-year return period.

109. The potential error from the curve fitting process can be best seen in plots of raw versus regressed output. For Fox Hill Drawbridge, the raw and the regressed still-water level stage-frequency curves, previously presented in Figure 35, had a linear regression correlation coefficient of $r = 0.997$. Figure 56 shows the raw versus regressed output for the "Wide Berm + 1-ft Cap" alternative at Roughans Point which had a correlation coefficient of $r = 0.994$. These correlation coefficients are representative of those occurring at all locations. The regression was highly accurate and potentially introduced only minor error into the total process. The lowest correlation coefficient was greater than 0.98 for both the still-water level locations and the interior of Roughans Point.

Determining Error Bands for the Selection Process

110. The selection process that determined which events were selected for modeling was designed specifically for this project. As a result of limited experience with this technique, it is much more difficult to determine the potential error of the selection process as compared to the potential error of the more familiar processes of data collection, data analysis, and numerical modeling. In order to estimate the variability of the selection

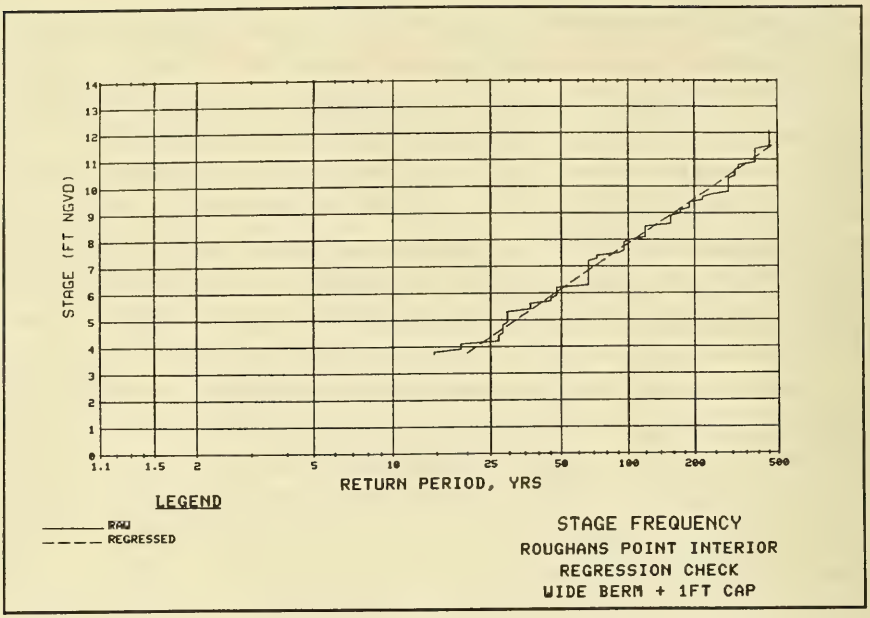

Figure 56. Raw and regressed stage-frequency curves, "Wide Berm + 1-ft Cap"

process, the 150 events were divided into three sets of 50 events each. Each of these sets was processed separately producing three stage-frequency curves. These three curves were generated for each numerical gage for the still-water level locations as well as for each of the six structure combinations at Roughans Point. As was mentioned in Part II, 150 events were more than necessary to produce consistent results for the still-water locations. This assertion was confirmed when stage-frequency curves derived separately from the three sets of 50 events were plotted for each still-water location. For most of the locations there was not a discernible difference between curves from the three sets. Figure 57 contains the three stage-frequency curves for Oak Island which had the greatest variation of all the still-water locations. As can be seen from this figure the variation resulting from selecting a limited number of events to represent all possible events is negligible for the still-water locations.

111. The potential error caused by the selection process is much greater for stage-frequency curves for the interior of Roughans Point than for the stage-frequency curves for the still-water level portion of this project. The flooding levels in the interior of Roughans Point are dependent not only upon

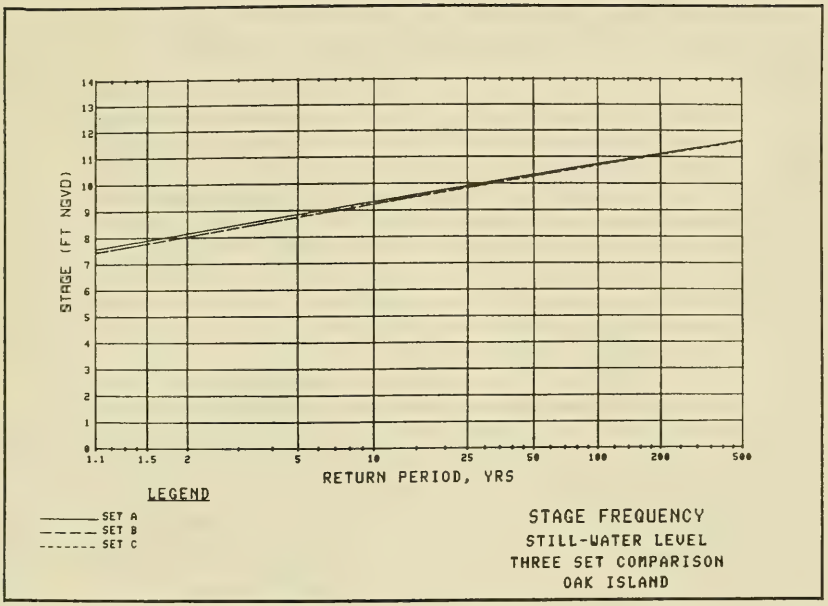

Figure 57. Stage-frequency curves, three-set comparison, Oak Island

the still-water level of the event but also upon the magnitude, direction, and duration of the event's waves. Since the selection process used still-water level as its only criterion, two events which were selected with the same still-water level could have very different wave characteristics and, therefore, could cause very different flood levels at Roughans Point. Stage-frequency curves for the three sets of 50 events are shown in Figures 58 and 59 for the "Wide Berm" and the "Wide Berm + 1-ft Cap" alternatives, respectively, which had the most and the least variation among the three sets, of any of the six Roughans Point structure combinations.

112. Assuming that for any given return period the calculated stage is a normally distributed random variable, an estimate of the probable error PE can be calculated using the three stage-frequency curves generated independently from the three sets of selected events. PE estimates the 50 percent error bounds about the mean value in a series of measurements. Equation 18 states the relationship between PE and standard deviation σ as

$$PE = 0.6745\ \sigma \tag{18}$$

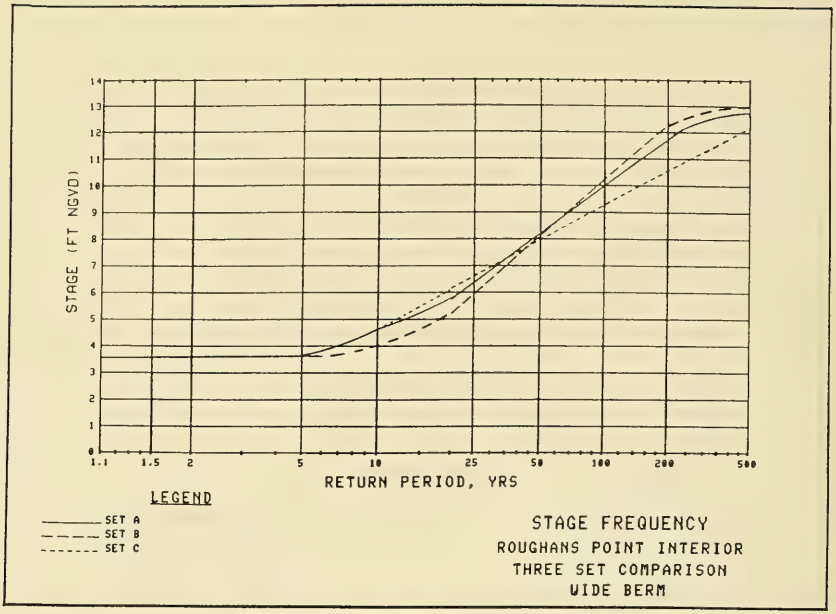

Figure 58. Stage-frequency curves, three-set comparison, "Wide Berm"

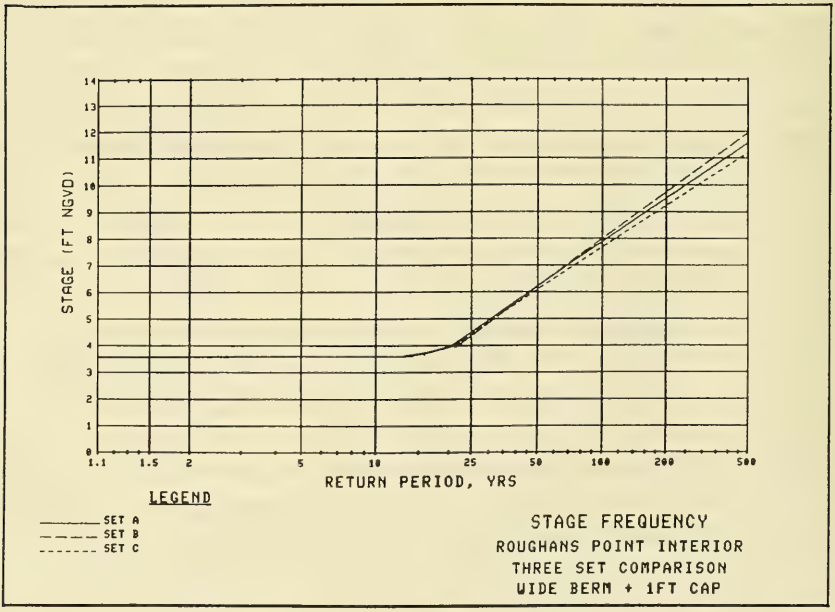

Figure 59. Stage-frequency curves, three-set comparison, "Wide Berm + 1-ft Cap"

Table 11 shows the relationship between the range of stages Ra calculated at any return period and σ, (Beyers 1966).

Table 11
Estimate of Standard Deviation from Range

Sample Size	Estimate of σ
2	0.8862 Ra
3	0.5908 Ra
4	0.4857 Ra

113. A single stage-frequency curve with probable error bands at selected return periods was produced using the following process. First, at each return period where error bounds were desired, the range of simulated stages was determined by ranking the three values and subtracting the smallest from the largest. Second, the PE was estimated using Table 11 and Equation 18. Third, a single curve was produced by processing all 150 events as one set using the methods discussed in Part VI. Finally, the PE bounds were placed upon this combined curve. Figures 60 and 61 show the combined curves with error bounds which correspond to the three curves shown in Figures 58 and 59, respectively. Probable error curves are not presented for any still-water locations. The probable error of the selection process is too small to be seen for the still-water locations because of the small variability shown in Figure 57.

Assessing the Impact of the Standard Project Northeaster

114. The Standard Project Northeaster (SPN) definition can be determined from the definition for the Standard Project Storm (Headquarters, Department of the Army, Office of the Chief of Engineers, 1952) as the northeaster which results from the "most severe combinations of meteorologic" and tidal "conditions that are considered reasonably characteristic of the geographical region involved, excluding extremely rare combinations." For this report two processes are important in considering the specification of an SPN, still-water level and wave overtopping. It is possible that a separate SPN would have to be defined for each process. The SPN which would produce the

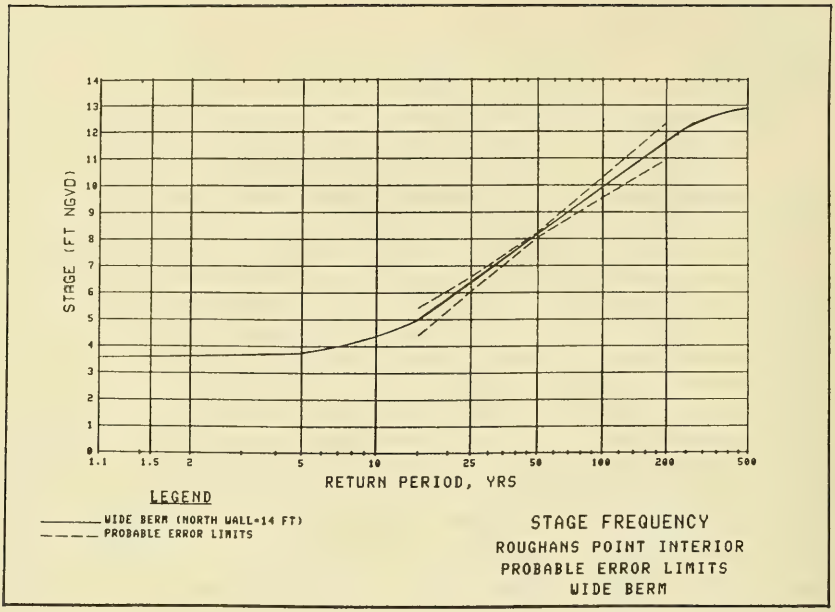

Figure 60. Probable error of the selection process, "Wide Berm"

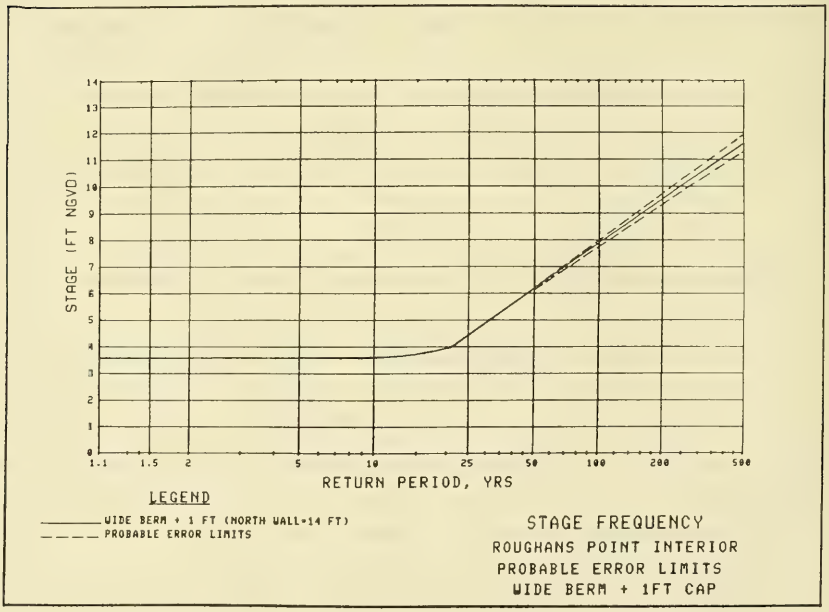

Figure 61. Probable error of the selection process, "Wide Berm + 1-ft Cap"

highest still-water level might not produce the highest waves at Roughans Point and, therefore, not the highest overtopping rates.

115. The SPN still-water level was estimated to be 13.0 ft NGVD (NED 1983) by adding the maximum surge recorded at Boston, about 5 ft, and the maximum probable tide, 7.4 ft NGVD and then rounding up to the next foot of elevation. This resulted in a still-water elevation which was almost 3 ft higher than the maximum ever recorded at the Boston gage. Given the unlikely event that a tide with a maximum elevation near the maximum probable tide were to occur sometime during the maximum surge producing northeaster, the probability that the hour of maximum surge (using hour increments) would occur at the hour of maximum tide is only 1/24 (assuming a semidiurnal tide with unequal highs). Consequently, this combination might fall under the "excluding extremely rare" clause in the definition of the SPN. A better specification of the SPN still-water level might be closer to 12.0 ft NGVD.

116. This report is mainly concerned with the effect of the SPN on interior flooding at Roughans Point and the propagation of the SPN still-water level throughout the study area which can be easily stated regardless of the exact specification of the SPN still-water level. In considering the interior floods at Roughans Point, the effect of an SPN is straightforward; the interior of Roughans Point would fill to overflowing. The interior water level (approximately 1-2 ft higher than the still-water level in Broad Sound) would be determined by how fast the overtopping volumes would flow over roadways at the west boundary of Roughans Point. The evidence seems clear that given a water level on the order of 12-13 ft NGVD and with the waves appropriate for an SPN, all of the proposed alternatives would be swamped. This can best be seen by considering Figure 36. The only alternative which offers significant protection at the highest return periods is the "Wide Berm + 2-ft Cap." However, even this alternative would not offer protection against the SPN. The highest still-water level (in Broad Sound) tested in the simulations was 11.2 ft, roughly a 500-year level. Although the SPN would fall well to the right of the edge of Figure 36, the effect of the SPN can be estimated as follows. The extra foot of still water resulting from the SPN would change a 2-ft cap down to an effective 1-ft cap. Furthermore, the larger and longer waves caused by the effect of deeper water in front of the structure and the higher wind speeds of the SPN would further increase the flood levels. Consequently, the interior levels caused by the SPN with the "Wide Berm + 2-ft

Cap" would be more severe than that shown for the "Wide Berm + 1-ft Cap" at the 500-year return period. It is possible that although the proposed improvements at Roughans Point would offer considerable protection against lesser northeasters, the flood levels for the SPN might be higher after the improvements. Without the improvements, water will begin returning to the ocean over the north wall at approximately 11 ft NGVD. This outflow of water considerably lessens the probability of extreme interior flood levels. With the improvements, this outflow would be prevented by the increased wall heights until much higher water levels. The lack of data to ascertain the relative importance of outflow over the walls versus the outflow at the western edge of the Roughans Point area at extreme interior flood levels makes definitive conclusions difficult.

117. For the still-water locations the numerical storm surge model results showed that the Broad Sound maximum water levels produced by the ensemble storms were efficiently conveyed throughout the Saugus-Pines River system. Differences between outside and inside water levels were always small with the inside level usually slightly higher. The time-history of the SPN surge might be more peaked. This peaked profile would likely suffer more loss through the inlet and channel system, but this loss would be offset by the local wind setup of the shallower water of the flood plain (the cause of the higher interior levels during the simulations). Therefore, the predicted result of the SPN still-water level would be that the whole study area would flood to the level of the SPN in Broad Sound.

Conclusions

118. Stage-frequency curves for 15 possible structure combinations at Roughans Point and for 14 still-water level locations were presented and discussed. The potential error associated with each step of the procedure was discussed. A more formal determination of the probable error of the selection process was presented. Finally the estimated impact of the SPN was discussed for both interior flooding at Roughans Point and the still-water locations.

119. At Roughans Point, where flooding is caused by the overtopping of seawalls by storm waves, physical, numerical storm surge, numerical wave, flood routing, and probability models were needed. Multiple combinations of possible seawall-revetment structures were modeled. Major differences among

the combinations were evident at the lower return periods with the combinations of a wide berm revetment and a cap on the existing seawall for the east wall of Roughans Point providing the greatest protection. At higher return periods the protection differential offered by the various structure combinations tends to diminish. For still-water levels and wave conditions of an SPN, all structure combinations tested would be ineffective at protecting the interior of Roughans Point. Tests were run to determine a structure height for the north wall. These tests indicated that significant overtopping did not begin until the north wall structure was lowered below 13 ft. Since the existing height of the north wall is above this level at several sections, it is recommended that the revetment height be set at 13 ft with the wall height being set so that there is a transition between the existing wall heights. The only height that would be raised would be that of wall D, which would be raised to match wall C.

120. For areas where flooding is due to coastal inundation by the still-water level resulting from the combination of storm surge and astronomical tide, only the storm surge and probability models were necessary. These areas include both open coast and estuarine locations. For these areas flooded by the still-water level, the results of the modeling indicated that the whole study area floods to approximately the same level. The flood levels are efficiently conveyed through the inlet and throughout the flood plain of the Saugus-Pines River system. Inside the inlet there is a small gradient in the still-water level, rising from north to south, which results from local wind setup caused by north to northeast winds which predominate during storm conditions. This local wind setup results in flood levels inside the inlet which vary by one-half to three-fourths of a foot during the more severe storm events. Outside the river system in Broad Sound a smaller north-south gradient exists with differences of only a few tenths of a foot resulting. Data collected after completion of the modeling indicated that losses do occur as the flood levels are conveyed upstream of the Fox Hill Drawbridge on the Saugus River and upstream of the Highway embankment on the Pines River. Stage-frequency curves for these areas were adjusted to accommodate these additional data. The curves were lowered 0.3 and 0.5 ft at the lower return periods for upstream Saugus River and Pines river locations, respectively. These reductions were linearly reduced for higher return periods because higher flood levels would provide greater access to these areas.

Ahrens, J. P., and Heimbaugh, M. S. In preparation. "Irregular Wave Overtopping of Seawall/Revetment Configurations, Roughans Point Massachusetts," Technical Report, US Army Engineer Waterways Experiment Station, Vicksburg, Miss.

Ahrens, J. P., and McCartney, B. L. 1975. "Wave Period Effect on the Stability of Riprap," Proceedings of Civil Engineering in the Oceans/III, American Society of Civil Engineers, pp 1019-1034.

Beyers, W. H., ed. 1966. Handbook of Tables for Probability and Statistics, The Chemical Rubber Company, Cleveland, Ohio. pp 270-272.

Butler, H. L. 1978. "Coastal Flood Simulations in Stretched Coordinates," Proceedings, 16th International Conference on Coastal Engineering, Hamburg, Germany.

_____. 1983. "Lake Pontchartrain and Vicinity Hurricane Protection Plan, Report 3, Numerical Model Investigation of Plan Impact On the Tidal Prism of Lake Pontchartrain," Technical Report HL-82-2, US Army Engineer Waterways Experiment Station, Vicksburg, Miss.

Corson, W. D., et al. 1981 (Jan). "Atlantic Coast Hindcast, Deepwater, Significant Wave Information," WIS Report 2, US Army Engineer Waterways Experiment Station, Vicksburg, Miss

_____. 1982 (Mar). "Atlantic Coast Hindcast Phase II, Significant Wave Information," WIS Report 6, US Army Engineer Waterways Experiment Station, Vicksburg, Miss.

Harris, D. L. 1981. "Tides and Tidal Datums in the United States," CERC Special Report No. 7, US Army Engineer Waterways Experiment Station, Vicksburg, Miss.

Headquarters, Department of the Army, Office of the Chief of Engineers. 1952. "Standard Project Flood Determinations," Engineer Manual 1110-2-1411, US Government Printing Office, Washington, DC.

Hubertz, J. M. 1985. "A Users Guide to a Steady-State Shallow-Water Directional Spectral Wave Model," Instruction Report CERC-86-1, US Army Engineer Waterways Experiment Station, Vicksburg, Miss.

Hughes, S. A. 1984. "The TMA Shallow-Water Spectrum, Description and Applications," Technical Report CERC-84-7, US Army Engineer Waterways Experiment Station, Vicksburg, Miss.

Jensen, R. E. 1983. "Methodology for the Calculation of Shallow-Water Wave Climate, WIS Report 8," US Army Engineer Waterways Experiment Station, Vicksburg, Miss.

Kitaigorodskii, S. A., Krasitskii, V. P., and Zaslavakii, M. M. 1975. "On Phillips' Theory of Equilibrium Range in the Spectra of Wind Generated Gravity Waves," Journal of Physical Oceanography, Volume 5, pp. 410-420.

Meyers, V. A. 1970. "Joint Probability Method of Tide Frequency Analysis Applied to Atlantic City and Long Beach Island, N. J.," ESSA Technical Memorandum WBTM HYDRO 11, US Department of Commerce, Environmental Science Services Administration, Weather Bureau, Silver Springs, Md.

Prater, M. D., Hardy, T. A., and Butler, H. L. In preparation. "Fire Island to Montauk Point, New York, Storm Surge Model Study," Technical Report, US Army Engineer Waterways Experiment Station, Vicksburg, Miss.

Shore Protection Manual. 1984. 4th edition, 2 volumes, US Army Engineer Waterways Experiment Station, Coastal Engineering Research Center, US Government Printing Office, Washington, DC.

US Army Engineer Division, New England. 1983. "Roughans Point, Revere, Massachusetts-Coastal Flood Protection Study, Interim Report," Vols I and II, Waltham, Mass.

Weggel, J. R. 1977. "Wave Overtopping Equation," Proceedings of the Fifteenth Coastal Engineering Conference, American Society of Civil Engineers, pp 2737-2755.

DOCUMENT
LIBRARY
Woods Hole Oceanographic
Institution

OCT 2 8 1986

GEMLO